1D interpretation of electromagnetic response estimates with the Psi-algorithm

Ulrich Schmucker, Goettingen

1 Preliminaries

There seem to be good reasons to return from time to time to 1-dimensional interpretations of electromagnetic (EM) sounding data. Not long ago Whittall & Oldenburg (1992) published an extensive treatise on the subject and Parker & Booker (1996) presented an extension of their earlier work to treat the 1D non-linear inversion without recourse to linearization. It is also interesting to note that still sites are singled out in the most complicated and multi-dimensional situations, where an interpretation by 1D models can be justified (e.g. Lathi et al., 2005; Section 4). It may not be very difficult anymore to find models which match EM sounding data within error limits, provided they are sufficiently consistent with this kind of interpretation. There will be, however, a multitude of competing models to account for a limited number of error-bearing estimates. Therefore the fit of modelled to observed responses should be only one of several criteria when interpreting EM sounding data. Other aspects are the structural complexity of the derived model, the achieved resolution at a given target depth and the accuracy of the model at that depth.

These four aspects will be the key elements of the following discourse. It is centred on the Psi-algorithm, of which Larsen (1975, Section 5.1) gave a concise outline, and a short overview can be found in Appendix A. Further references are Schmucker (1974), Schmucker & Weidelt (1975, Section 6.4) and Haak (1978, Section 3.12), here in connection with related work by Eckhardt (1968). Subsequent improvements have been summarized by Schmucker (2001). They are extended now and complemented.

2 The linearization of the 1D inverse problem

We seek to formulate a well-posed inverse problem in the sense that its solution depends continuously on the data. Otherwise small changes of the data, by errors for example, could yield quite disparate solutions. For instance, when $\tau(z) = \int_0^z 1/\rho(\hat{z})\, d\hat{z}$ denotes the depth-integrated conductivity, with z as depth and ρ as resistivity, then the derivation of $\tau(z)$ from EM responses represents a well-posed problem, and the same presumably applies when deriving $\rho(z')$ in a conductivity-weighted depth

$$z'(z) = \int_0^z \sqrt{\rho_0 / \rho(\hat{z})}\, d\hat{z} \qquad (1)$$

(Weidelt, 1972; eq.4.2), while the derivation of $\rho(z)$ in true depth would be ill-posed (Berdichevsky & Dmitriev, 2002; Sections 8.1 and 8.3). The transition from z to z' implies that depth sections of high resistivity, in comparison to ρ_0, are compressed and those of low

resitivity enlarged, smoothing out the downward attenuation of the incident field. The scaling constant ρ_0 can be freely chosen, but should lie preferably in the range of expected resistivities as inferred for instance from the range of apparent resistivities (cf. Appendix B).

When a continuous model $\rho(z')$ in z'-depth is approximated by a sequence of layers of resistivity ρ_m (m=1,2,..,M-1) above a uniform half-space of resistivity ρ_M, we shall subdivide it into layers of *constant* thickness d'. Eq. (1) implies then that the model $\rho(z)$ in true depth has the layer thicknesses

$$d_m = d'\sqrt{\rho_m / \rho_0}\,, \tag{2}$$

a constraint which has been uses repeatedly in the past in this context. It implies that only the layer resistivities remain as the *M* unknowns to be found, provided the layer thickness d' is not among them, as it will be the case in our approach. The optimal choice of d' will be considered separately in Subsection 4.4.

Under certain circumstances, when for example the responses to be interpreted extend over a wide range in frequency and thereby over a large range of penetration depths, it may be useful to follow Larsen (1975) and to vary layer thicknesses also in z' by adopting layer weights w_n relaxing the above constraint to

$$d_m = w_n \cdot d'\sqrt{\rho_m / \rho_0}\,. \tag{3}$$

In this way the model can be more finely subdivided at shallow depths than further down, for example, concentrating then on the interpretation of high frequencies, or vice versa. The weights are either arbitrarily chosen or determined separately in an iterative process, which starts with preliminary layer resistivities derived for unit weights. Then by solving a linear system similar to that in the forthcoming eq. (4), successive improvements are obtained simultaneously for w_n as well as ρ_m.

The data to be interpreted are complex-valued transfer functions for angular frequency ω_n, with $n = 1,2,..,N$. Henceforth we denote them with y_n, the layer parameter for resistivity to be found with x_m, with $m = 1,2,..,M$ and the connecting non-linear functional for the *n*-th frequency with F_n. Constraining layer thicknesses according to eq. (2), the functional depends in addition to the layer parameter only on the layer thickness d' multiplied with the frequency factor α_n as introduced in the forthcoming eq. (6), yielding in $y_n^{\mathrm{mod}} = F_n(x_1, x_2, ..., x_M; \alpha_n d')$ the model response for frequency ω_n. Unless the non-linear 1D problem is truly to be solved by inversion, an iterative procedure can be used by linearization of the problem. A standard, but here not followed form of linearization proceeds from a Taylor expansion of the functional, truncated after first-order terms: $y_n = F_n(x_m^{(0)}; \alpha_n d') + \sum_m \frac{\partial F_n}{\partial x_m}\Delta x_m$ with the derivatives taken at $x_m = x_m^{(0)}$ and with $x_m^{(0)}$ as starting model. The resulting linear problem

$$y_n - F_n(x_m^{(0)}; d') = \sum_m \frac{\partial F_n}{\partial x_m} \Delta x_m^{(0)} + \delta(y_n - F_n), \tag{4}$$

with $\delta(..)$ as misfit residual, is solved towards improvements $\Delta x_m^{(0)}$. They are added to the starting model to yield $x_m^{(1)}$ for the next iteration and new derivatives of F_n at $x_m = x_m^{(1)}$. The iterations may or may not converge towards a final model, not counting the possibility that it may be influenced by the choice of the starting model. But the principal drawback for our purposes is that modelling errors are difficult to obtain, and thus they are rarely quoted in the literature for models which have been derived in this manner.

The use of the Psi-algorithm resolves partially the convergence problem and removes the other two shortcomings altogether. Data and model are defined now in such a way that the functional receives the quasi-linear form

$$y_n^{\mathrm{mod}} = \sum_m g_{nm} x_m, \tag{5}$$

with g_{nm} as data kernel (cf. eq. A4), which depends primarily on the preset product $\alpha_n d'$, to a lesser degree also on the model parameter x_m, thus preserving the non-linearity of the inverse problem. But the dependence on layer resistivity is weak unless the model is very rugged. When for example resistivity changes between adjacent layers over two orders of magnitude, with $0.1 \le \rho_{m+1}/\rho_m \le 10$, the data kernel does not change by more than about 10%. Furthermore, no starting model is involved because iterations can start with the totally model-independent approximation

$$g_{nm}^{(0)} = 2\sinh(\alpha_n d') \exp(-2\alpha_n z'_m) \quad \text{with} \quad \alpha_n = \sqrt{i\omega_n \mu_0 / \rho_0} \tag{6}$$

and $z'_m = (m - 1/2)d'$ as depth of the centre of the *m*-th layer in z' (cf. eq. A5). Solving then the linear problem

$$y_n = \sum_m g_{nm}^{(0)} x_m^{(1)} + \delta y_n, \tag{7}$$

it yields in $x_m^{(1)}$ for $m = 1,2,..,M$ a first model approximation. The calculations are repeated with the exact data kernel $g_{nm}^{(1)}$ for this model, leading to a second approximation $x_m^{(2)}$, and so on until the differences of misfit residuals δy_n in consecutive iterations fall below a pre-set threshold. In this way each iterative cycle generates a completely new model, while updating the data kernel concurrently from cycle to cycle. Thus model errors as they arise from data errors are readily derived for the final model. The remaining problem of convergence will be addressed in Subsection 4.5. After the first iteration it is also possible to change to spherical models and to derive the first set of exact data kernels accordingly.

Depending on whether 1D sounding experiments are conducted with geomagnetic time variations alone or in combination with those of the geoelectric field, the pertinent EM responses for angular frequency ω_n are the C-response $C(\omega_n)$ or the magneto-telluric impedance $Z(\omega_n)$, with $Z(\omega_n) = i\omega C(\omega_n)$. Converted into apparent resistivities and phases

of impedance we obtain $\rho_a(\omega_n) = \mu_0/\omega_n \cdot |Z(\omega_n)|^2 = \mu_0\omega_n \cdot |C(\omega_n)|^2$ and $\varphi(\omega_n) = \arg\{Z(\omega_n)\}$ $= \arg\{C(\omega_n)\} + \pi/2$. As shown in Appendix A, the following definition of data and model leads to the desired quasi-linear form of the functional:

$$y_n = 2 \cdot [\ln\{C(\omega_n)/C_0(\omega_0)\}] = \ln\{\rho_a(\omega_n)/\rho_0\} + 2i\{\varphi(\omega_n) - \pi/4\} \tag{8}$$

with $C_0(\omega_n) = 1/\alpha_n$ as C-response of a uniform half-space of resistivity ρ_0, while the natural logarithm of resistivity in the form

$$x_m = \ln\{\rho_m/\rho_0\} \tag{9}$$

defines the model parameter. Eq. (8) is identical with Parker & Booker's eqs 4 and 5 (1996), even though here in a very different context. Estimation errors $\Delta C(\omega_n)$ for $|C(\omega_n|$ yield data error $\Delta y_n = 2\Delta C(\omega_n)/|C(\omega_n)|$. Equating in the usual way $\Delta\rho_a/\rho_a$ with the phase error, Δy_n is also the error of the real and imaginary parts of y_n.

Renamed u_m, also an alternative model parameter will be used in order to express the change of resistivity from layer to layer,

$$u_m = \ln(\rho_m/\rho_{m-1}) = x_m - x_{m-1} \tag{10}$$

with $x_0 = 0$ and

$$y_n^{\mathrm{mod}} = \sum_m \hat{g}_{nm}\, u_m \tag{11}$$

as functional. The model-independent approximation of the new data kernel $\hat{g}_{nm}$ to start iterations is

$$\hat{g}_{nm}^{(0)} = \exp\{-2\alpha_n(z'_m - d'/2)\} \tag{12}$$

(cf. eq. A7 and A8).

3 The pseudo-inverse of the data kernel

We continue in vector and matrix notations. presuming that their components and elements are real-valued. Since complex data and thereby complex data kernels have been used so far, the first N positions of the data vector $\underline{y}$ are filled with the real part and the following N positions with the imaginary part of the data, proceeding in the same way when filling the $2N$ rows of the $2N \times M$ data kernel matrix $\underline{\underline{G}} = (g_{nm})$. Without change of notations y_n represents henceforth for $n \le N$ the real part of the data, as defined in eq. (8), and for $n > N$ the imaginary part, and the same shall apply to the data kernel.

Under certain circumstances it can be of advantage to interpret only apparent resistivities or only phases. Omitting then the first or the second N entries, the data vector is reduced to N components and the data kernel matrix to N rows. Otherwise the interpretation is performed in

exactly the same way. When only phases are interpreted, the scaling resistivity ρ_0 can be used to match modelled and observed apparent resistivity for some selected frequency, thus giving the model absolute scales in resistivity and depth.

Let now $\underline{x} = (x_1, x_2, .., x_M)^T$ denote the model vector. Then without reference to the respective iteration, eq. (7) reduces with $\underline{\delta y}$ for the real and imaginary part of the misfit residual to

$$\underline{y} = \underline{\underline{G}} \cdot \underline{x} + \underline{\delta y} \,. \tag{13}$$

A direct inversion of $\underline{\underline{G}}$ in the case of $2N = M$ will not be considered any further because the solution $\underline{x} = \underline{\underline{G}}^{-1} \cdot \underline{y}$ leaves no room for misfit residuals and is thereby unrealistic for error-bearing data. Instead a pseudo-inverse $\underline{\underline{H}}$ of $\underline{\underline{G}}$ will be used with dimensions $M \times 2N$. Applied to the data vector $\underline{y}$ the solution of eq. (13) becomes

$$\underline{\bar{x}} = \underline{\underline{H}} \cdot \underline{y} \,. \tag{14}$$

The *k*-th components of thus obtained model vector $\underline{\bar{x}}$ represents in

$$\bar{x}_k = \sum_{m=1}^{M} a_{km} x_m \tag{15}$$

a certain average over layers which are adjacent to the *target* layer $m = k$, with $k = 1,2,..,M$. The coefficients a_{km} are elements of a so-called $M \times M$ resolution matrix $\underline{\underline{A}}$. Combining eq. (14) with eq. (15) in vector notations yields $\underline{\underline{H}} \cdot \underline{y} = \underline{\underline{A}} \cdot \underline{x}$, and with $\underline{y} = \underline{\underline{G}}\underline{x}$ we obtain $\underline{\underline{A}} = \underline{\underline{H}} \cdot \underline{\underline{G}}$ and thus

$$a_{km} = \sum_{n=1}^{2N} h_{kn} \, g_{nm} \tag{16}$$

to express the resolution coefficients in terms of solution coefficients and data kernel. A similarly derived $2N \times 2N$ information density matrix $\underline{\underline{B}} = \underline{\underline{G}} \cdot \underline{\underline{H}}$ connects in $\underline{y} = \underline{\underline{B}} \cdot \underline{y}^{\mathrm{mod}}$ the empirical and model responses. Both matrices can be thought to apply certain filter operations on model and data, as outlined in Appendix B.

When data of very unequal quality are involved and none of them is to be totally rejected, weights $s_0 / \Delta y_n$ can reduce the influence of bad data with large errors Δy_n, i.e. y_n is replaced by $y'_n = s_0 / \Delta y_n \cdot y_n$ and the data kernel g_{nm} by $g'_{nm} = s_0 / \Delta y_n \cdot g_{nm}$, for consistency, with a corresponding change of solution coefficients to h'_{kn}. All weighted data have now the same error s_0, where $s_0 = 1$ is a common choice. We shall use the harmonic mean of the errors instead. Then with unity as mean weight, bad data receive weights below unity and good data those above unity, while preserving in s_0 an indicator for the errors of the original data. A further reason for using the harmonic mean will become transparent in Subsection 5.2.

Eq. (14) implies that the k-th component of the resolvable model vector is

$$\vec{x}_k = \sum_{n=1}^{2N} h_{kn} y_n \qquad \text{or} \qquad \vec{x}_k = \sum_{n=1}^{2N} h'_{kn} y'_n , \tag{17}$$

depending on whether original or weighted data are interpreted. It follows readily that the quadratic error or variance of $\vec{x}_k$ due to data errors is

$$\Delta\vec{x}_k^2 = \sum_n h_{kn}^2 \Delta y_n^2 \qquad \text{or} \qquad \Delta\vec{x}_k^2 = s_0^2 \sum_n h_{kn}'^2 , \tag{18}$$

provided that the individual errors $\Delta y_{n\ell} = y_{n\ell} - y_n$ of the analysed time sections $\ell = 1,2,..,L$ are independent in the sense that the sums of products $\Delta y_{n\ell} \cdot \Delta y_{\hat{n}\ell}$ over all sections are zero for $n \neq \hat{n}$.

For completeness we summarize the singular value decomposition of the data kernel matrix, which leads to the definition of its pseudo-inverse (cf. for example Kress, 1991; Section 5). Let $p \leq \min(M,2N)$ be the maximum number of rows and columns of a non-singular quadratic matrix, which can be fitted into the rectangular matrix $\underline{\underline{G}}$, if necessary with a prior re-arrangement of rows and columns to maximize *p*. Let μ_j with $j = 1,2,..,p$ denote the *p* positive eigenvalues of the eigenvalue problems $\underline{\underline{G}}^T \underline{\underline{G}}\, \underline{v}_j = \mu_j \underline{v}_j$ and $\underline{\underline{G}}\,\underline{\underline{G}}^T \underline{u}_j = \mu_j \underline{u}_j$, ordered according to size, and let the $M \times p$ matrix $\underline{\underline{V}}$ and the $2N \times p$ matrix $\underline{\underline{U}}$ be the modal matrices of eigenvectors $\underline{v}_j$ and $\underline{u}_j$, respectively. Then the singular value decomposition of the data kernel is $\underline{\underline{G}} = \underline{\underline{U}}\,\underline{\underline{\Lambda}}\,\underline{\underline{V}}^T$, yielding in $\underline{\underline{H}} = \underline{\underline{V}}\,\underline{\underline{\Lambda}}^{-1}\underline{\underline{U}}^T$ its pseudo-inverse, where $\underline{\underline{\Lambda}}$ is a diagonal $p \times p$ matrix containing the so-called *singular values* $\lambda_j = +\sqrt{\mu_j}$ as elements.

The thus obtained pseudo-inverse does not provide, however, a realistic solution in our context because eigenvalues up to $j = \min(M,2N)$ are never exactly zero, even though they might be very small. Assuming then $p = \min(M,2N)$, we obtain least squares or minimum-norm solutions of purely over-determined or under-determined linear systems. They are Gauss' least squares solution

$$\underline{\underline{H}} = (\underline{\underline{G}}^T \underline{\underline{G}})^{-1} \underline{\underline{G}}^T \tag{19}$$

for $p = M < 2N$, which minimizes $\underline{\delta y}^T \underline{\delta y}$ for the best possible fit between empirical and modelled responses, and the minimum-norm solution

$$\underline{\underline{H}} = \underline{\underline{G}}^T (\underline{\underline{G}}\,\underline{\underline{G}}^T)^{-1} \tag{20}$$

for $p = 2N < M$, which minimizes $\underline{\vec{x}}^T \underline{\vec{x}}$ giving the least rugged model. The first pseudo-inverse yields a perfectly resolved model with $\underline{\underline{A}} = \underline{\underline{I}}_M$, the second provides a model which perfectly explains the data with $\underline{\underline{B}} = \underline{\underline{I}}_{2N}$. But as a rule, the normal equation matrix $\underline{\underline{G}}^T \underline{\underline{G}}$ or $\underline{\underline{G}}\,\underline{\underline{G}}^T$ is ill-conditioned for inversion. The resulting models are thus very sensitive against

data errors and the often extreme changes of resistivity from layer create convergence problems for the iterative process.

The thereby expressed adverse effect of small eigenvalues can be avoided by adding a damping factor γ_j to the reciprocals of λ_j. The choice of Tikhonov's $\gamma_j = \lambda_j^2/(\alpha + \lambda_j^2)$, with $\alpha > 0$, and thereby the replacement of $\underline{\underline{\Lambda}}^{-1}$ by $(\alpha \underline{\underline{I}}_{p\times p} + \underline{\underline{\Lambda}}^2)^{-1}\underline{\underline{\Lambda}}$ in the singular value decomposition of $\underline{\underline{H}}$, eliminates the need for decomposition altogether, leading to the thus defined regularized least squares and minimum-norm solutions

$$\underline{\underline{H}} = (\underline{\underline{G}}^T \underline{\underline{G}} + \alpha \underline{\underline{I}}_M)^{-1} \underline{\underline{G}}^T \tag{21}$$

and

$$\underline{\underline{H}} = \underline{\underline{G}}^T (\underline{\underline{G}}\,\underline{\underline{G}}^T + \alpha \underline{\underline{I}}_N)^{-1} \ . \tag{22}$$

They neither minimize the model misfit nor the model norm anymore. Furthermore, none of the matrices $\underline{\underline{A}}$ or $\underline{\underline{B}}$ remains unitary and the resulting model is less resolved than without regularisation. But model oscillations are suppressed and model errors reduced. The identity

$$(\underline{\underline{G}}^T \underline{\underline{G}} + \alpha \underline{\underline{I}}_M) \cdot \underline{\underline{G}}^T = \underline{\underline{G}}^T \cdot (\underline{\underline{G}}\,\underline{\underline{G}}^T + \alpha \underline{\underline{I}}_N),$$

when multiplied with $(\underline{\underline{G}}\,\underline{\underline{G}}^T + ...)^{-1}$ from the right and then with $(\underline{\underline{G}}^T \underline{\underline{G}} + ...)^{-1}$ from the left shows that for $\alpha > 0$ the solution matrices $\underline{\underline{H}}$ in eqs (21) and (22) are identical. They are presented here separately only to illuminate their connection to the pseudo-inverses without regularisation. The regularisation parameter α could be chosen, for example in the way that the iterations converge toward a model structure which appears as significant in terms of errors. We shall use a different approach, however, and shall use α to constrain either the model norm or the misfit residual norm.

4 The preparation and conduct of 1D model interpretations

4.1 Consistency test

Before entering into details about the actual procedures of model construction, a number of points have to be considered. First of all the data set may be at least partially inconsistent with the intended interpretation, i. e. no layered model exists which could reproduce it completely. If the causes are large random errors, still a smoothed-out model can be derived by regularization. But in the case of well determined estimates, regularisation is no substitute for the then possibly required interpretation with multi-dimensional models. Weidelt's inequalities (1972, eqs 2.30-2.34) provide straightforward tests for consistency. The constraints for phases, in $0 \le \varphi(\omega_n) \le \pi/2$, and for the slope of apparent resistivity curves, in $|d(\ln \rho_a)/d(\ln T_n)| \le 1$ with period $T_n = 2\pi/\omega_n$, are rather weak and rarely violated. More stringent is the condition for the real part of the C-response $z^*(\omega_n) = \mathrm{Re}\{C(\omega_n)\}$ as indicator for the depth of penetration. In $dz^*/dT_n \ge 0$ this condition implies that penetration depths may not decrease, when periods increase. Violations are readily detected, for example, in the

form of loops in $\rho^* - z^*$ presentations of the data. Other not so easily detectable violations concern condition for the first and second derivatives of the complex-valued C-response. Guidelines for their implementations can be found in Weidelt (1986).

4.2 Static shifts of magneto-telluric apparent resistivities

Otherwise well determined magneto-telluric data are distorted frequently by near-surface anomalies. But they may remain consistent with 1D models, separately for the two polarisation of the magnetic field, provided that the distortion is quasi-static and the surrounding regional structure 1-dimensional. The second condition can be tested with a dimensionality study of the impedance tensor. It may show that at least a limited period range exists, within which 1D modelling towards the regional structure is justified (e.g. Bibby et al. ,2005; Fig.6). There is no need to remove the distortion prior to the interpretation. Quasi-static distortion means that within the allowed period range apparent resistivities for the off-diagonal elements of the impedance tensor are multiplied with unknown shift-factors *g* with respect to their undistorted values, with different factors for the two polarisations. In our data definition according to eq. (8) static shift merely implies that $\ln(g)$ is added to the real parts of y_n, which is equivalent to changing the scaling resistivity ρ_0 to a different value $\rho_0' = \rho_0 / g$. As shown in Appendix B this has no effect upon the modelling results, provided d' is changed to $d'' = d' \cdot \sqrt{\rho_0 / \rho_0'}$. Hence, an interpretation of apparent resistivities for the two polarisations as they are, alone or together with phases, yields two separate, but presumably similar models for the regional structure, even though without absolute scaling for depth and resistivity. When the shift factors were somehow known, then multiplying depths with $\sqrt{1/g}$ and subtracting $\ln(g)$ from $\ln(\rho_m / \rho_0)$ would provide also absolute scaling.

4.3 The choice of the regularisation parameter

Except for rare cases 1D interpretations require regularisation, and the problem arises which regularisation parameter α to chose. When a singular value decomposition of the data kernel matrix has been performed and thus the range of eigenvalues is known, α can be chosen in order to dampen effectively the influence of small eigenvalues. Otherwise the choice is quite arbitrarily and, for example, α could be given a large enough value that the iterative process for finding a model converges. Here we shall adopt, however, a different *target-oriented* approach by constraining either the model norm or the misfit norm. Thus either $|\underline{\vec{x}}|^2$ or $|\underline{\delta y}|^2$ should match a pre-set constraining constant *c*. The interpretations are started then with an arbitrarily chosen value α_0. Using Newton's method the interpretation is repeated with $\alpha_1 = \alpha_0 - (s - c) \cdot (\partial s / \partial \alpha)^{-1}$, where *s* denotes one of the squared norms. Appendix C shows how to calculate the differential quotient $\partial s / \partial \alpha$. Interpretations are carried out with the thus updated value α_1, and they are repeated until the target $s = c$ is reached.

4.4 The choice of the layer thickness *d'*

For a successful 1D interpretation it is essential to subdivide the model $\rho(z')$ in an optimal manner into layers of constant thickness d', particularly when sparsely subdivided models

with few layers are considered. Ideally the penetration depths $z^* = \mathrm{Re}(C)$ of the responses should fit evenly into the range from $z' = 0$ to $z' = M \cdot d'$. But the transfer of z^* into z'-depths would involve the not yet known resistivities. Therefore the following pragmatic procedure has been adopted: For given values of M and α, a starting value for d' is chosen which is definitely too small. Thus, the iterative process will derail after a few iterations because changing model parameter of excessive size violate the assumption of only weakly model-dependent data kernels. The calculations are repeated with a gradually increased d' until iterations start to converge and continued until divergence sets in again. Within the range of convergence $|\underline{\delta y}|^2$ will have a more or less well developed minimum, and the value of d', where this minimum occurs, will be regarded as optimal. The whole procedure is repeated with changing regularisation parameter, when pursuing the above stated target. The remaining problem how to find the right number of layers is postponed until Subsection 4.6.

4.5 The divergence problem

Divergence of the iterative process occurs when interpreting inconsistent or poorly determined response estimates, also for an improperly chosen layer thickness d'. In either case model parameter of excessive and rapidly changing size overstrain the basic concept of the chosen form of linearization that data kernels should not change much from one iteration to the next. Hence, iterations should be stopped, when $|x_m|$ in any layer exceeds a certain limit. With 6.9 as limit, for example, ρ_m / ρ_0 may vary over six orders of magnitude. In principle divergence could be overcome by limitless regularisation. But the result would be flattened out models of little meaning.

4.6 The derivation of sparsely subdivided models

We are ready now to turn to the actual conduct of 1D interpretations, for which two principal options exist. When the fit of model responses to empirical responses has first priority, then with $M < 2N$ the pseudo-inverse of eq. (21) for an over-determined linear system represents the right choice because it minimizes in $|\underline{\delta y}|^2$ the model misfit norm. Mostly no regularisation or only a modest regularisation is required to ensure convergence. As a consequence sparsely subdivided models are always well resolved. In cases where regularisation is needed, the regularisation parameter α is used to control the model norm with the condition $|\underline{x}|^2 = c$. Since this norm is determined mainly by the largest positive or negative model parameter, a choice of, say, $c = 6.9^2$ allows ρ_m / ρ_0 to vary over roughly three orders of magnitude.

In view of the limited number layers the optimal choice for the layer thickness d' is critical and the constraint placed on layer thicknesses should be relaxed as described in the context of eq. (2). For deciding on the right value of M, misfit residuals are derived for an increasing number of layers, using each time the optimal choice for d'. Starting with very few layers, the residuals will gradually become smaller as the number of layers grows and as soon as this decline levels off the optimal number of layers is reached. Near this limit also more than one minimum of $|\underline{\delta y}|$ can appear, indicating the existence of equivalent models with the best resolution either at shallow or at great depth. Models with a limited number of layers may or may not resemble reality. They can be appropriate in the case of geological strata with different resistivities and sharp boundaries, or for an Earth's mantel, in which resistivity is controlled by phase transitions rather than by a gradually changing temperature.

4.7 The derivation of finely subdivided models

When smoothness of a quasi-continuous model has the first priority, the minimum-norm solution of an under-determined linear system with $2N < M$ will be appropriate according to eq. (22). It is then preferable to use as model parameter not the logarithmic resistivity itself, but its logarithmic change from layer to layer. Thus we change from model parameter x_m to model parameter u_m of eq. (10) with a concurrent change of the data kernel from g_{nm} to $\hat{g}_{nm}$. Once the new model parameter and their errors have been found, models in terms of logarithmic resistivities and their errors follow from

$$\vec{x}_k = \sum_{\ell=1}^{k} \vec{u}_\ell \qquad \text{and} \qquad \Delta\vec{x}_k = \sum_{\ell=1}^{k} \Delta\vec{u}_\ell \,. \tag{23}$$

Regularisation is now always required, while controlling with the regularisation parameter the misfit norm. Since the data should be neither under-interpreted nor over-interpreted, the appropriate condition to be satisfied is $|\underline{\delta y}|^2 = \sum_n \Delta y_n^2$. If weighted data $y'_n = s_0 / \Delta y_n \cdot y_n$ are interpreted, the condition simplifies to $|\underline{\delta y'}|^2 = 2N \cdot s_0^2$. When data errors have been underestimated or when data with well determined errors are inconsistent with 1D models, it may not be possible to lower the squared misfit norm to the desired level, and the condition has to be relaxed to $|\underline{\delta y'}|^2 = q\,2N \cdot s_0^2$, where $q > 1$ is some properly chosen constant.

With $M > 2N$ there exists no upper limit for the number of layers, but increasing it beyond any reasonable limit does not improve resolution which always should be taken into consideration. Hence, it suffices to select M as to give the model a quasi-continuous appearance, while the selection of a suitable thickness d' is not any longer critical.

In the limit of a truly continuous model, with $d' \to dz'$ and $u_m = x_m - x_{m-1} \to dx(z')/dz'$ for $M \to \infty$, the minimum-norm solution minimizes in $|dx/dz'|^2$ the derivatives of the logarithmic resistivity with respect to the conductivity-weighted depth z'. Translated into true depth with $dz' = \sqrt{\rho_0 / \rho(z)}\, dz$ according to eq. (1), the minimized squared model norm is $|\sqrt{\rho/\rho_0}\ \rho^{-1} d\rho/dz|^2$. In this sense the finely subdivided models belong to the class of minimum gradient models. Constable et al. (1987) introduced the denomination of *Occam-models*, when they are derived with a minimum of assumptions and thus with the smallest measure of arbitrariness. In our understanding not only the finely subdivided models should be regarded as Occam-models, but also the sparsely subdivided models, when as outlined the number of layers as well as the position of layer boundaries is required by the data.

5 Resolution and model accuracy

So far we have used *global* criteria when deriving models, i.e. the misfit norm involves the residuals of *all* frequencies and the model norm the model parameter of *all* layers. In contrast resolution and accuracy represent *local* criteria because they concern modelling result only for a specified target layer $m = k$ or target depth z'_k. Even though it would be possible to derive for this layer or depth a best resolved or best determined model or a combination of both, this will not be our primary goal. Instead we seek to formulate solutions, which when applied to

hypothetical data with *hypothetical* errors would yield a *hypothetical* model in accordance with the just described local criteria.

5.1 Models with the best possible resolution

The first task is to define a measure for resolution, which when brought to a minimum provides the best achievable resolution for a given target layer or target depth. We consider two options. The first measure, here defined for discrete models, is

$$D_k = \sum_m (a_{km} - \delta_{km})^2 , \tag{24}$$

with $\delta_{km} = 1$ for $k = m$ and zero otherwise. This measure approaches zero, when for perfect resolution $a_{km} \to \delta_{km}$. The second measure is an averaging length

$$\Delta_k = \sum_m a_{km}^2 \, J_{km} , \tag{25}$$

again in the formulation for discrete models . This second measure is the key element of the Backus & Gilbert (B&G) theory, in which Δ_k indicates the width or *spread* of the depth range, over which the model is averaged (cf. for example Schmucker & Weidelt, 1975; Section 6.1 or Parker, 1996; Section 4.02). In eq. (25) it is defined as a dimensionless number for a spread in units of d'. The factor J_{km} involves the squared distance $|m-k|$ between the m-th layer and the target layer in order to bring the resolution coefficients a_{km} as closely as possible to those for a perfect resolution.

We start with the problem to find the minimum of D_k and return for a moment to the singular value decomposition. We note that in $\underline{\underline{A}} = \underline{\underline{H}}\,\underline{\underline{G}} = \underline{\underline{V}}\,\underline{\underline{V}}^T$ a connection is established between resolution and the eigenvectors $\underline{v}_j$. Utilizing their orthogonality, we expand the rows of $\underline{\underline{A}}$ in terms of the components of $\underline{v}_j$ and seek expansion coefficients β_{kj} in $a_{km} = \sum_{j=1}^{p} \beta_{kj} v_{mj}$ which minimize D_k. Setting the derivatives of D_k with respect to β_{kj} for $j = \hat{j}$ to zero gives

$$\frac{\partial D_k}{\partial \beta_{k\hat{j}}} = 2 \sum_m \{ \sum_j \beta_{kj} v_{mj} - \delta_{km} \} v_{m\hat{j}} = 0 ,$$

which with $\sum_m v_{mj} v_{m\hat{j}} = \delta_{j\hat{j}}$ reduces to $2(\beta_{k\hat{j}} - v_{k\hat{j}}) = 0$ or $\beta_{k\hat{j}} = v_{k\hat{j}}$. The resulting coefficients $a_{km} = \sum_m v_{kj} v_{mj}$ are readily identified as the elements of the matrix product $\underline{\underline{A}} = \underline{\underline{V}}\,\underline{\underline{V}}^T$ in the *k*-th row and *m*-th column. This shows that any pseudo-inverse leads to a solution of minimum D_k and in this sense to models of maximum resolution, regardless of other minimizing criteria. The least squares solution of eq. (19) has to be exempted, since it implies $D_k = 0$.

For reasons which will be come transparent soon, we turn to an alternative way to minimize D_k by substituting the resolution coefficients a_{km} in eq. (24) according to eq. (16).

Proceeding as before, now with derivatives towards the solution coefficients h_{kn} at $n=\hat{n}$, we obtain

$$\frac{\partial D_k}{\partial h_{k\hat{n}}} = 2\sum_m (\sum_n (h_{kn}\, g_{nm} - \delta_{km}) \cdot g_{\hat{n}m} = 0 \,,$$

for $\hat{n}=1,2,..,2N$. After division by two and after changing the sequence of summations the resulting minimum condition for D_k is

$$\sum_n h_{kn} \sum_m g_{nm}\, g_{\hat{n}m} - g_{\hat{n}k} = 0 \quad . \tag{26}$$

We identify the sum over *m* readily as the element of the matrix product $\underline{\underline{G}}\,\underline{\underline{G}}^T$, as it appears in eq. (20), for the *n*-th row and $\hat{n}$-th column. Rewriting this equation in the form $\underline{\underline{H}}\;\underline{\underline{G}}\,\underline{\underline{G}}^T = \underline{\underline{G}}^T$, the explicit expression for the *k*-th row reproduces eq. (26) in

$$\sum_n h_{kn} \sum_m g_{nm}\, g_{\hat{n}m} = g_{\hat{n}k} \;.$$

This verifies the conclusion from above for the special case of an un-regularized minimum norm solution which fully explains the data.

The B&G theory is based on the same preposition that a model exists which can reproduce the data without misfit residual. Substituting then in eq. (25) the coefficients a_{km} again with the aid of eq. (16), the minimum of the spread is found by differentiation of Δ_k towards h_{kn} for $n=\hat{n}$, leading to $\frac{\partial \Delta_k}{\partial h_{k\hat{n}}} = 2\sum_m \sum_n h_{kn}\, g_{nm}\, g_{\hat{n}m}\, J_{km} = 0$ or

$$\sum_n h_{kn} \sum_m g_{nm}\, g_{\hat{n}m}\, J_{km} = 0 \tag{27}$$

for $\hat{n}=1,2,..,2N$. We note that except for the added factor J_{km} and zero right-and-sides, the minimum condition of the spread corresponds to the minimum condition for D_k in eq. (26). In order to obtain a system of inhomogeneous equations, B&G add the condition $\sum_m a_{km} = 1$ similar to the constraint applied to numerical filters. Thus when the model is uniform with x_m equal to some constant x_c, the averaged model parameter $\bar{x}_k = x_c \sum_m a_{km}$ $_c$ is correctly x_c.

We regard now the model $x(z') = \ln\{\rho(z')/\rho_0\}$ to be a continuous function of depth z', thereby following the B&G theory in its original formulation. But since we continue with discrete data, eq. (17) remains valid, now yielding averages $\bar{x}_k$ of $x(z')$ for a specified target depth z'_k. With $d' \to dz'$, $g_{nm} \to G_n(z')\,dz'$ and $a_{km} \to A_k(z')dz'$ we replace eq. (7) in real notations by

$$y_n = \int_0^\infty G_n(z')\, x(z')\, dz' \;, \tag{28}$$

without allowance for a misfit residual. Furthermore

$$\bar{x}_k = \int_0^\infty A_k(z')dz' \qquad \text{and} \quad A_k(z') = \sum_n h_{kn} G_n(z') \tag{29}$$

take the place of eqs (15) and (16), with $\int_0^\infty A_k(z')\,dz' = 1$ as condition for the now continuous resolution function $A_k(z')$. The definition of the spread is changed in correspondence to eq. (25) to

$$\Delta_k = \int_0^\infty \{A_k(z')\}^2 J_k(z')\}dz' \tag{30}$$

and the minimum condition of eq. (27) for the spread to

$$\sum_n h_{kn} \int_0^\infty G_n(z') G_{\hat{n}}(z') J_k(z')\,dz' = 0\,. \tag{31}$$

It is not intended to conduct an iterative process, in which the data kernel $G_n(z')$ is adapted iteratively to a sequence of model approximations. Therefore we shall use here exclusively the model-independent approximation

$$G_n^{(0)} = 2\alpha_n \exp(2\alpha_n z') \tag{32}$$

as it follows readily from eq. (6), here with its real part for $n \le N$ and its imaginary part for $n > N$, noting that the data kernel as well as the resolution functions are now dimensioned quantities. Evaluation of the condition for $A_k(z')$ with this approximation gives with the aid of eq. (29)

$$\int_0^\infty A_k(z')\,dz' = \sum_n h_{kn} \int_0^\infty G_n^{(0)} dz' = \sum_n h_{kn} = 1 \tag{33}$$

after changing the sequence of integration and summation. In the case of layered models the sum $\sum_m g_{nm}$ over the data kernels is always unity, as shown in Appendix B, whether or not they are approximated, leading in

$$\sum_m a_{km} = \sum_n h_{kn} \sum_m g_{nm} = \sum_n h_{kn} = 1 \tag{34}$$

to the same result. Differentiation of these conditions with respect to h_{kn} for $n = \hat{n}$ gives unity and thus the term to be added to the minimum conditions in eqs (27) and (31) is solely a Lagrange multiplier λ_k. Thus altogether we have $2N+1$ linear equations for the same number of unknowns, $2N$ solution coefficients h_{kn} and one Lagrange multiplier. These equations are

$$\sum_n h_{kn} b_{n\hat{n}} + \lambda_k = 0 \text{ for } \hat{n} = 1,2,..,2N \quad \text{and} \quad \sum_n h_{kn} = 1 \tag{35}$$

with

$$b_{n\hat{n}} = d' \sum_m g_{nm}\, g_{\hat{n}m}\, J_{km} \qquad \text{or} \qquad b_{n\hat{n}} = \int_0^\infty G_n(z')\, G_{\hat{n}}(z')\, J_k(z')\, dz' .$$

In the case of a discrete model the layer thickness d' has been added as a factor to obtain in either case a dimensioned spread. In the case of a continuous model the integral can be solved analytically with the model-independent approximation $G_n^{(0)}$ from eq. (32), while for discrete models we can use either the approximation $g_{nm}^{(0)}$ of eq. (6) or the exact data kernel for a preconceived model.

It remains to decide upon the factors J_{km} and $J_k(z')$. The B&G theory recommends to use the quadratic form $J_k(z') = c \cdot (z' - z'_k)^2$, whereas a suitable value for the constant c is obtained as follows: Suppose we have a delta-shaped resolution function, which is zero outside a small depth range of width $\Delta z'$ and inside this range $1/\Delta z'$ to meet the condition for $A_k(z')$. It is then reasonable to require that Δ_k equals $\Delta z'$ which yields $c = 12$. Translated to the discrete case the requirement is that the dimensioned Δ_k should be equal to the layer thickness d', which leads to $J_{km} = 1 + 12 \cdot (m-k)^2$.

The system of linear equations can be solved with standard methods and obviously the solution has to be repeated for each chosen target layer or target depth, even though the factors J_{km} and $J_k(z')$ are the only quantities, which vary. Numerical stability should be of no concern. EM responses which are suitable for a 1D interpretation cover rarely more than one or two decades in frequency, with ten estimates per decade at the most. Once the $2N$ solution coefficients h_{kn} and the Lagrange multiplier have been found, an averaged model parameter could be derived according to eq. (17). But unless exact data kernels for a preconceived model have been used to determine the coefficients $b_{n\hat{n}}$ in eq. (35), such models are of limited value unless they would provide a starting model for a here not intended iterative process. Much more relevant are the model variances as provided by eq. (18). There is no need to calculate the spread Δ_k from its respective definition because, as shown in Appendix D, it is identical with the Lagrange multiplier except for the sign.

Turning now to the resolution, we have to distinguish between continuous and discrete models. In the second case resolution coefficients are readily determined according to eq. (16). For continuous models we subdivide the model space into *M* depths segments of equal width $\Delta z'$, which is small enough to approximate the resolution function sufficiently well, while *M* should be large enough to allow a fairly complete display of this function, which tends to zero with increasing downward distance from the target depth. For each depth segment we define now a mean value of the data kernel

$$\bar{G}_{nm} = \frac{1}{\Delta z'} \int_{z'_m - \Delta z'/2}^{z'_m + \Delta z'/2} G_n(z')\, dz'$$

with z'_m again as the depth of the centre of the *m*-th depth segment, and the integration can be carried analytically with the approximated data kernel of eq. (32), Then a corresponding mean value of the resolution function follows from eq. (29) as

$$\bar{A}_{km} = \sum_n h_{kn} \bar{G}_{nm} , \tag{36}$$

which is the equivalent of a_{km} / d' for layered models.

5.2 Models with the smallest possible variance

The determination of models of minimum variance $\Delta\bar{x}_k^2$ is a quite simple matter. Assuming that all data have the same error s_0, the differentiation of the relevant eq. (18) with respect to h_{kn} for $n = \hat{n}$ gives

$$2 s_0^2 h_{k\hat{n}} + \lambda_k = 0 \quad \text{for } \hat{n} = 1,2,..,2N , \tag{37}$$

which implies that the solution coefficients are the same for all $\hat{n}$ and, in view of eqs (33) and (34), we obtain $h_{kn} = 1/2N$. This leads in a straightforward manner to the minimum value of the model variance

$$\Delta\bar{x}_k^2 = s_0^2 / 2N , \tag{38}$$

the same for all target layers or target depths, which reflects in $\Delta\bar{x}_k = s_0 / \sqrt{2N}$ the propagation law of errors. The determination of the not so easily found spread Δ_k is dealt with separately in Appendix D. It is readily seen that eq. (38) remains valid for a data set with non-zero variable errors Δy_n, when we insert for s_0 their harmonic mean $2N / \sum_n \Delta y_n^{-1}$.

5.3 Trade-off models between resolution and accuracy

Model resolution and model accuracy are conflicting criteria, when data errors are taken into account, i. e. when a well resolved model cannot be very exact at the same time, and vice versa. In fact models for minimum spread Δ_k are models with the greatest variance $\Delta\bar{x}_k^2$, and again vice versa. The B&G theory employs therefore a dimensionless trade-off parameter *w* in [0,1] and seeks now the minimum of a linear combination of spread and variance, with $w = 1$ for minimum spread and $w = 0$ for minimum variance. Combining then eqs (35) and (37), the $2N + 1$ linear equations to be solved for $w > 0$ are

$$w \sum_n h_{kn} b_{n\hat{n}} + (1 - w)\, s_0^2 h_{k\hat{n}} + \lambda_k = 0 \ \text{ for } \hat{n} = 1,2,..,2N \quad \text{and} \quad \sum_n h_{kn} = 1 . \tag{39}$$

We can proceed as in Subsection 5.1 to determine the model variance and the resolution coefficients, while Δ_k follows now from a combination of the Lagrange multiplier and the model variance, as shown again in Appendix D.

A visual display of this balanced interpretation is provided by so-called trade-off curves, which for a selected target layer or target depth show $\Delta\vec{x}_k$ in dependence of Δ_k, with w as curve parameter decreasing from unity to zero. These curves start at $w=1$ for the best possible resolution, associated with maximum and unacceptable modelling errors, and all curves merge at $w=0$ into the same minimum model error according to eq. (38), associated with a maximum and equally unacceptable spread. Very instructive are displays of trade-off curves for a sequence of target depths to visualize the decrease of resolution with increasing depth (cf. Fig. 6). They demonstrate also that a small sacrifice in resolution reduces modelling errors dramatically. Otherwise no fixed rules exist how to select an optimal trade-off parameter. A possible choice will be presented in connection with Fig. 4.

6 Demonstrations and comments to the figures

6.1 1D model interpretations with the six harmonics of daily variations

The various methods to derive models and to consider their resolution will be applied now to sets of empirical and hypothetical EM responses. We shall start with those for the six harmonics of daily variations. These are C-responses, obtained with the gradient method for the observatory Fuerstenfeldbruck in Southern Germany (cf. the contribution " Ein Kontinent erwacht …." in this volume). They are converted into data y_n according to eq. (8). The scaling resistivity is set to $\rho_0 = 70\Omega\,\mathrm{m}$, and thereby conductivity-weighted (z') and true depths (z) will not be too different within the first few hundreds kilometres below the Earth's surface. Penetration depths $z^* = \mathrm{Re}(C)$ reach from 332 km for the sixth harmonic (T=4 hrs) to 660 km for the first harmonic (T=24 hrs), thus setting the frame for constructing models. For completeness the following table includes also apparent resistivities ρ_a and ρ^* as well as phases φ. With $\varphi > \pi/4$ throughout the formula $\rho^* = 2\omega\mu_0\,\mathrm{Im}(C)^2 = 2\rho_a \cdot \cos^2\varphi$ applies. The decline of ρ^* from close to $100\Omega\,\mathrm{m}$ for the sixth harmonic to about $4\,\Omega\,\mathrm{m}$ for the first harmonic indicates the range of model resistivities which to expect. Numbers below the tabular entries are errors at the 95% confidence level.

Period	C-response	App. Resistivity ρ_a & ρ^*		Phase φ	Logarithmic response
24 hrs	$660-151i$ *km*	41.9 Ωm	4.2 Ωm	77.1 degr	$y_1 = -0.513+1.121i$
	(17)	(2.2)	(0.9)	(1.4)	(0.052)
12 hrs	$546-251i$	66.0	23.0	65.3	$y_2 = -0.058+0.709i$
	(13)	(2.9)	(2.4)	(1.2)	(0.043)
8 hrs	$463-244i$	75.1	32.6	62.2	$y_3 = +0.070+0.601i$
	(16)	(4.6)	(4.3)	(1.8)	(0.061)
6 hrs	$393-244i$	78.2	43.5	58.2	$y_4 = +0.111+0.460i$
	(26)	(8.8)	(9.3)	(3.2)	(0.112)
4.8 hrs	$386-257i$	98.3	60.4	56.3	$y_5 = +0.339+0.396i$
	(53)	(22.5)	(24.9)	(6.6)	(0.229)
4 hrs	$332-276i$	102.2	83.5	50.3	$y_6 = +0.378+0.184i$
	(62)	(29.4)	(37.5)	(8.2)	(0.287)

The monotonic increase of penetration depths with increasing period as well as the smooth change of ρ^* with period suggests that the data are consistent with 1D models. **Figs 1** and **2** present four equivalent models of different design, including their errors. The models to the left are sparsely subdivided and the models to the right finely subdivided, with the objectives

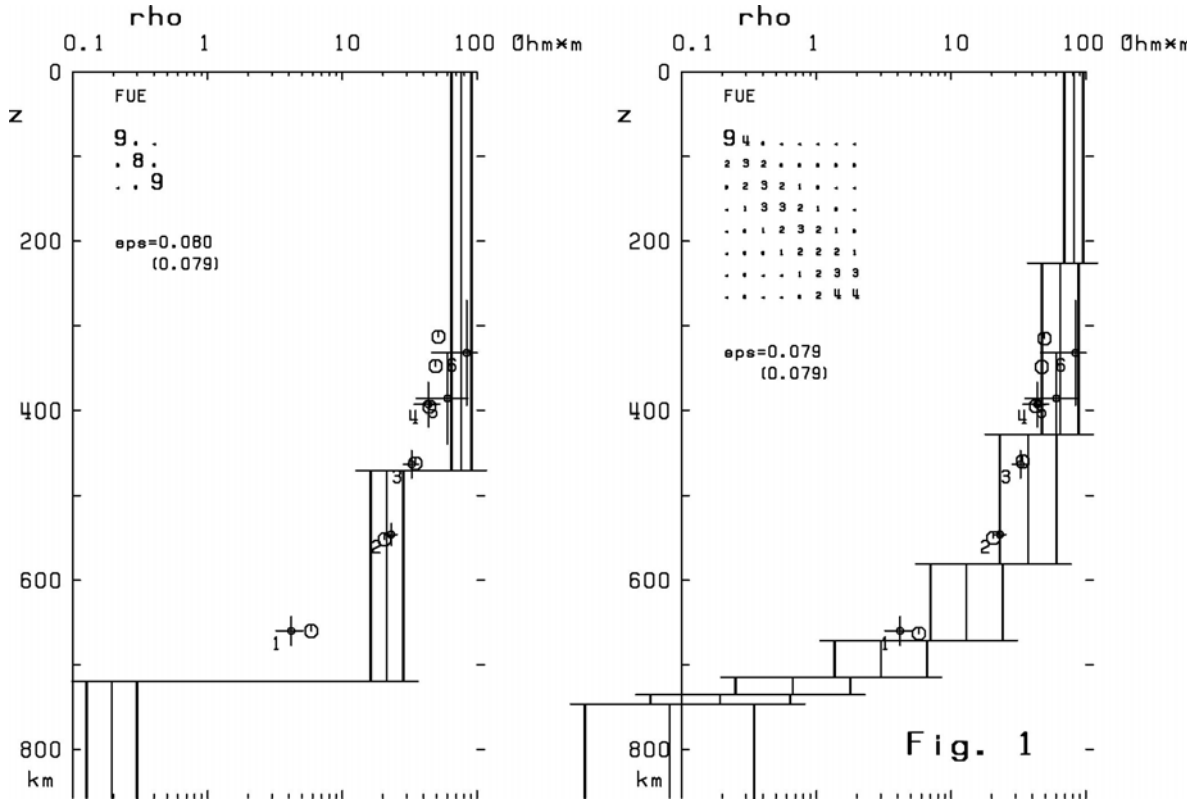

Fig. 1

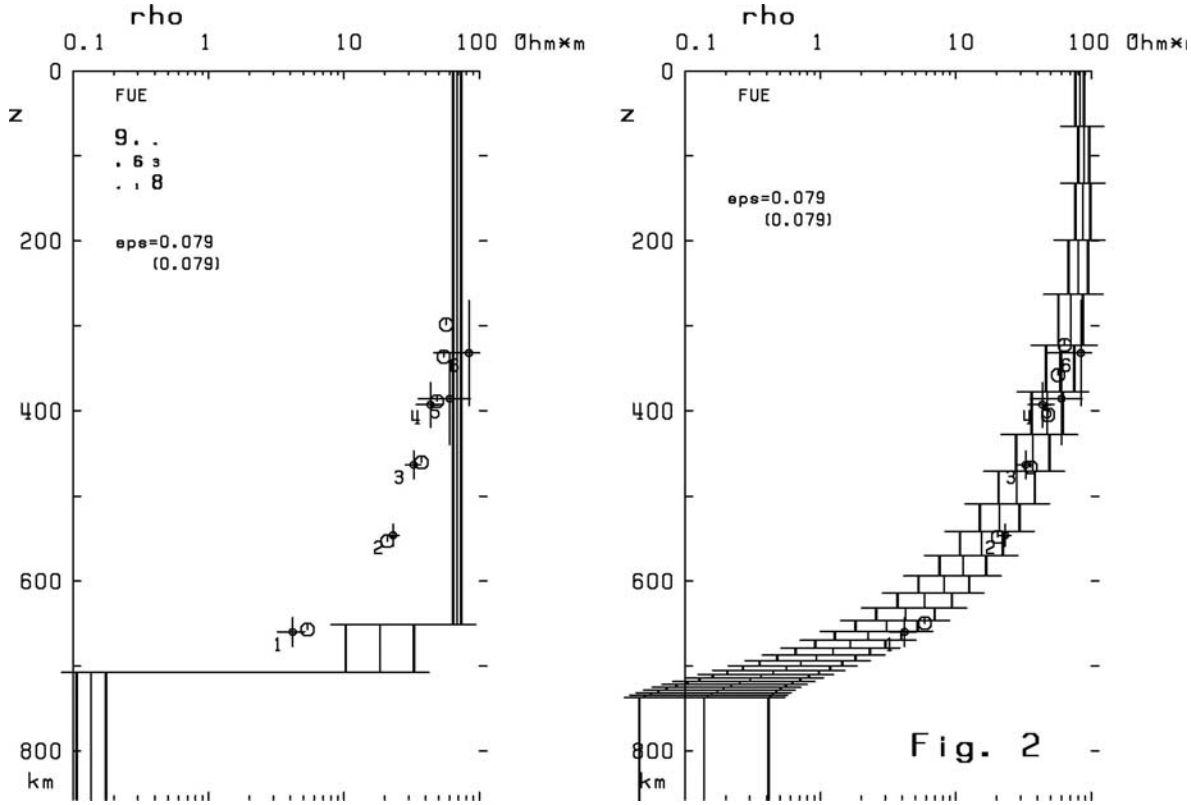

Fig. 2

as outlined in Subsection 4.6 and 4.7. It has been found that in the first case three layers are sufficient to account for the empirical estimates. An increase to more layers would not improve the model fit, while the best fitting 2-layer model has substantially greater misfit residuals, recalling that these are least squares models directed towards the best fitting model.

In Fig.1 layer boundaries are in accordance with eq. (2), i. e. the ratio $d_m / \sqrt{\rho_m}$ is kept constant, in Fig.2 they have been optimized with layer weights according to eq. (3), without reducing however the misfit residuals to any significant extent, as it will be seen. Both 3-layer models show step-wise reductions of resistivity from 90 Ωm at the top to 0.1-0.2 Ωm below 700 km depth, where the underlying uniform substratum begins, but in the model with variable layer weights the decline occurs in a narrow depth range between 650 and 700 km. In either case very moderate regularisation is required to ensure convergence of the iterative process, and the regularisation parameter α has been adjusted to limit layer resistivities to three orders of magnitude.

The models on the right are regularized minimum norm models with up to 32 layers. They provide the expected smoothed image of the 3-layer models, moving also the steep ascent downward to a fairly narrow depth range beneath a rather structure-less upper mantel. Furthermore, the increase from eight to 32 layers does not reveal any additional structural details except for a marginally significant intermediate maximum of ρ beneath the top layer.

Small full circles with error bars in the displays are the six empirical responses in a $\rho^* - z^*$ presentation, and the large open circles without error bars are the $\rho^* - z^*$ values for the model at the same frequency, thus visualizing in one single illustration the degree of fit between empirical and model responses together with the model itself. Numbers below to the left indicate the harmonics and thus frequencies in cycles per day (cpd). The arrays of numbers in the upper left corner represent resolution matrices $\underline{\underline{A}}$. As a visual aid coefficients $a_{km} \geq 0.9$ are shown as bold-faced large numbers **9**. With decreasing size of the coefficients numbers get thinner and smaller until they become very small and faint zeroes for $a_{km} < 0.1$. These arrays verify that the sparsely subdivided models are indeed well resolved. Top layer and substratum show an almost perfect resolution, while for the second layer between 60 and 80 % of the shown model resistivity come from the true resistivity of this layer itself. In the 8-layer model also the top layer and to some extent the substratum appear as well resolved, while for the layers in-between 70-80% of the displayed model resistivities arise from true resistivities in the target layer and the two layers next to it, leaving 20-30% for contributions from a greater distance. Since it would be impossible to present in the same way the resolution matrix of a 32-layer model, it will be shown separately in Figs 5 and 6, even though for two target depths only.

The two numbers below the resolution matrices are the rms misfit residual $\varepsilon_{\mathrm{mod}}$ and, in parenthesis, the rms data error ε_{dat}:

$$\varepsilon_{\mathrm{mod}} = \sqrt{\sum_n |\delta y_n|^2 / 2N} \quad \text{and} \quad \varepsilon_{dat} = \sqrt{\sum_n \Delta y_n{}^2 / 2N} \tag{40}$$

or $\varepsilon_{dat} = s_0$, when weighted data have been interpreted as it is done here. With $\Delta y = 2 \cdot \Delta C / |C| = \Delta\rho_a / \rho_a$ an rms data error of 0.079 implies that the responses have been determined with accuracies of about 8% for ρ_a and 4% for $|C|$, while an rms misfit residual of the same size means that model responses account for 92% of ρ_a and for 96% of $|C|$. The intentional exact agreement of $\varepsilon_{\mathrm{mod}}$ and ε_{dat} has been achieved by adjusting the regularisation parameter α accordingly. A better model fit could have been easily obtained by less

regularisation, leading to a more structured model, but then with a model misfit below the level of data errors.

We conclude that all four models explain the data equally well, and it is not possible to say, which one conforms better to reality. They may be regarded as uniquely determined models within their specified frame of construction. There will exist, for example, no other 8-layer or 32-layer regularized minimum norm model, in terms of logarithmic resistivity changes from layer to layer, which could produce also equality of $\varepsilon_{\mathrm{mod}}$ and ε_{dat}., and with $M \to \infty$ an equally unique continuous minimum gradient model in terms of $|\sqrt{\rho/\rho_0}\ \rho^{-1} d\rho/dz|^2$ would evolve.

6.2 Resolution curves for 1D models obtained from hypothetical EM responses

We shall investigate now the resolving power of EM responses quite generally, that is in terms of the data kernels for the frequencies involved and without specifying any particular data set or model. Depending on whether we assume the hypothetical models to be continuous or discrete, either mean values $\bar{A}_{km}$ of the resolution functions $A_k(z')$ or ratios a_{km}/d' are plotted versus depth $z' = z'_m$ which is the depth of the centre of the *m*-th depth segment, to which these resolution measures belong. All segments have the same thickness $\Delta z'$ and, when discrete models are considered, they extend uniformly downward to $M\,d\,z' = 1920$ km depth. Unless stated otherwise all calculations are carried out with model-independent approximate data kernels $G_n^{(0)}(z')$ and $g_{nm}^{(0)}$ according to eqs (32) and (6), while $\Delta z'$ is chosen to produce a sufficiently smooth appearance of the resulting resolution curves to approximate $A_k(z')$. They are shown for two exemplary target depths z'_k. For reasons which will become transparent soon, we shall use as target depths 270 km for the upper part of the hypothetical models and 570 km for their lower part. Areas below the resolution curves are unity or at least close to unity.

We start with considering the resolution, which can be achieved with the six harmonics of daily variations. **Fig. 3** on the left shows the resolution coefficients for a discrete minimum norm model *without* regularisation, i. e. eqs (26) have been solved towards solution coefficients h_{kn} which when inserted into eq. (16) yield the displayed ratios a_{km}/d' for $d' = 20$ km. They are compared on the right with mean values $\bar{A}_{km}$ for a continuous minimum spread model, deriving this time the solution coefficients from eqs (35) and subsequently the mean values from eq. (36). Arrows mark the respective target depth and the number below in parenthesis gives the spread in kilometres as derived from eq. (D3). In both cases we assume error-free data.

As it may have been expected, the minimum norm model has the best resolution, but on the expense of prominent negative side lobes. Since a severely under-determined system of linear equations has been solved, with $N = 12$ data against $M = 1920/20 = 96$ unknowns, the resulting presumably strongly oscillating model would be unrealistic anyhow. The minimum spread model has a substantially lower resolution at target depth, but no negative side lobes appear, even though there exist small oscillations near to the surface and at great downward distances form the target depth. But the resulting B&G model would be quite realistic and sufficiently stable against data errors, as it will be demonstrated in the next illustration. It should be noted that Fig. 3 shows the highest resolution which can be achieved with six

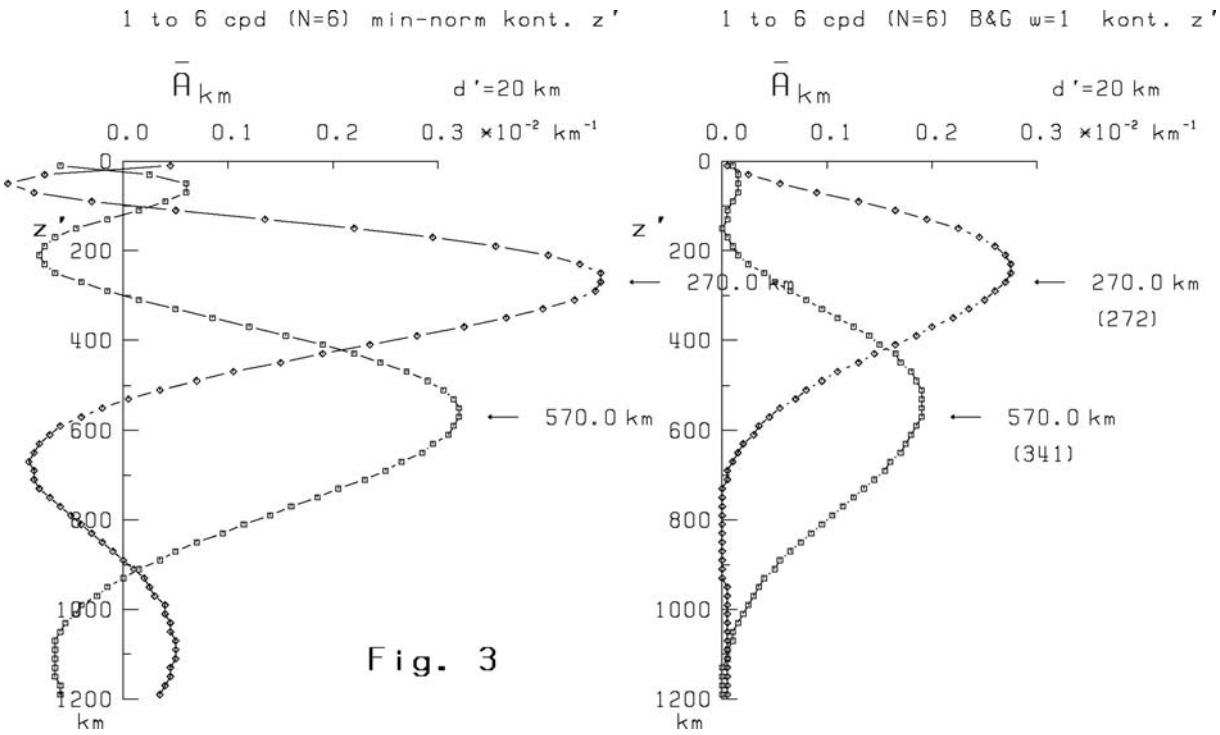

Fig. 3

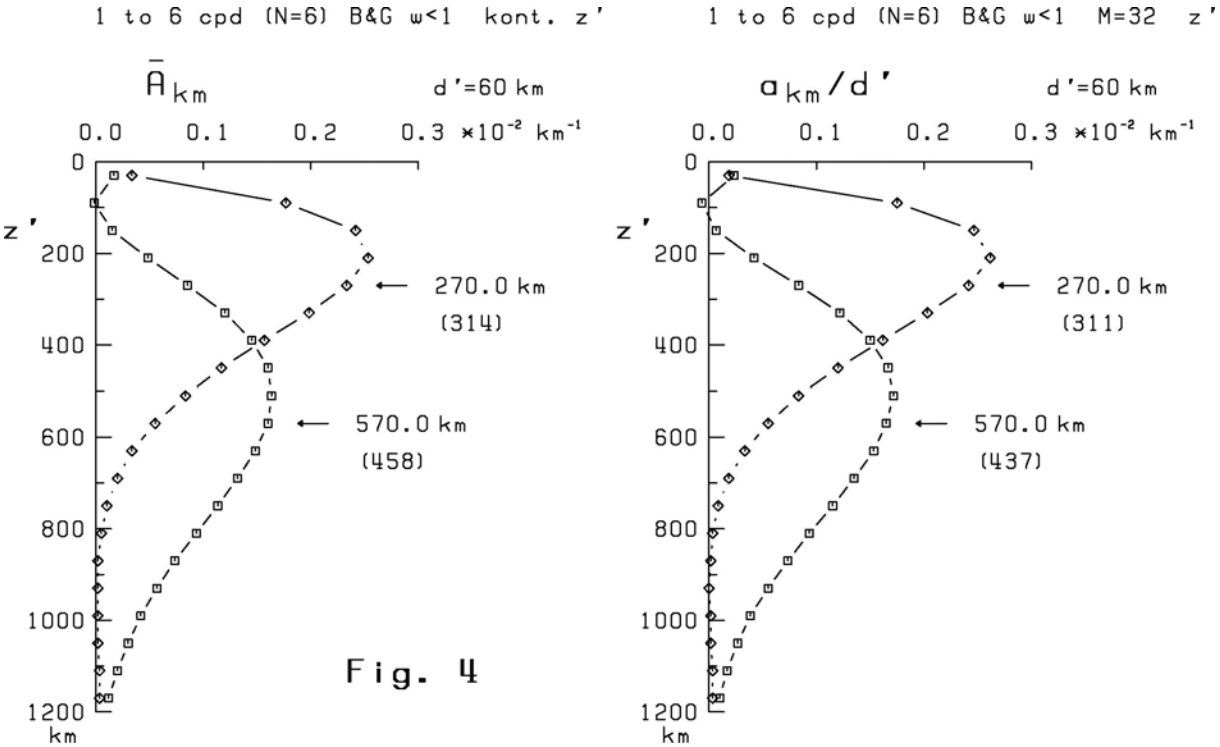

Fig. 4

responses from 1 cpd to 6 cpd, either in terms of minimum spread in the Backus-Gilbert theory or in terms of minimum D_k as defined in to eq. (24). For the upper part of the resulting hypothetical model we obtain a spread of 272 km and for its lower part a spread of 341 km, indicating that even under these most favourable conditions no small-scale structures can be resolved within the Earth's mantle.

Fig. 4 repeats the B&G resolution curve in Fig. 3 on the right, but now with the allowance of errors. Hence, they represent the resolution of trade-off models according to Subsection 5.3, i.e. eqs (39) have been solved, while Δ_k has been derived from Eq. (D2). The critical choice

of the trade-off parameter *w* has been as follows. With $\Delta z' = 60$ km and $M = 32$ the sequence of depth segments corresponds to the sequence of layers in the 32-layer model of Fig. 2 which has the same layer thickness $d' = 60$ km. In this way the two target depths are the centres of the fifth and tenth layer of this model, respectively. Then *w* is chosen to reproduce *exactly* the model errors $\Delta\vec{x}_k$ in these layers. The complete trade-off curves follow in Fig. 7. Resolution curves on the left refer as before to a continuous model, while those on the right to a discrete 32-layer model. It is comforting to see that this change has no marked effect, neither on the appearance of resolution curves or on their spread. Furthermore, the inclusion of data errors of 4% for $|C|$ or 8% for ρ_a has no dramatic effect either, with moderate increases of Δ_k from 272 to 314 km and from 341 to 458 km, respectively.

The left display in **Fig. 5** repeats Fig. 4 on the right, but now with the *exact* data kernels for the 32-layer model of Fig.2. It is again reassuring to note that also this modification does not lead to any significant changes in resolution and spread, demonstrating that studies of this kind with model-independent data kernels are quite adequate, without need for preconceived models. But under special circumstances this conclusion may have to be re-considered as shown towards the end of this subsection. The presentation on the right contains the resolution coefficients a_{km} for $k = 5$ and $k = 10$ as targets in the 32-layer model of Fig. 2. Since this is a minimum norm model, even though now *with* regularisation, it is not surprising to observe negative values towards the surface and towards greater downward distances from the target depth, even though they are not as conspicuous and regular as in Fig. 3 on the left. Otherwise the two pairs of resolution curves in Fig. 5 agree quite well, which means that regularized minimum norm and B&G trade-off models have quite comparable resolutions, provided that the choices of the parameter α and w are appropriate and compatible with each other.

So far resolution curves have been shown versus a conductivity-weighted depth z'. In order to obtain a more comprehensible display, the resolution curve on the left of Fig. 5 is shown again in **Fig .6,** but now as a function of true depth. The transfer from z' to z depths has been carried out with the resistivities of the 32-layer model. Hence, the spacing of coefficients is slightly increased within the first layers, where ρ_m exceeds ρ_0, while the resolution curve becomes more and more compressed towards greater depth and declining layer resistivites until they end at about 750 km. Hence, EM responses for daily variations cease to yield information about mantel resistivities beyond this depth, exceeding the penetration depth z^* of the first harmonic by nearly 100 km.

For completeness Fig. 6 shows on the right trade-off curves of model errors $\Delta\vec{x}_k$ versus spread Δ_k, assuming again a continuous model. Arrows mark those points, where the model errors $\Delta\vec{x}_k$ match those of the 32-layer model at the same target depth and we note that the chosen form of regularisation for this model has produced an optimal compromise between model resolution and accuracy. Very impressive is the steep decline of model errors, when Δ_k is moved slightly away from its minimum, while for $w \to 0$ both curves merge into the same ultimate model error, here $0.023 = 0.079/\sqrt{12}$ according to eq. (38) with $s_0 = 0.079$ as data error.

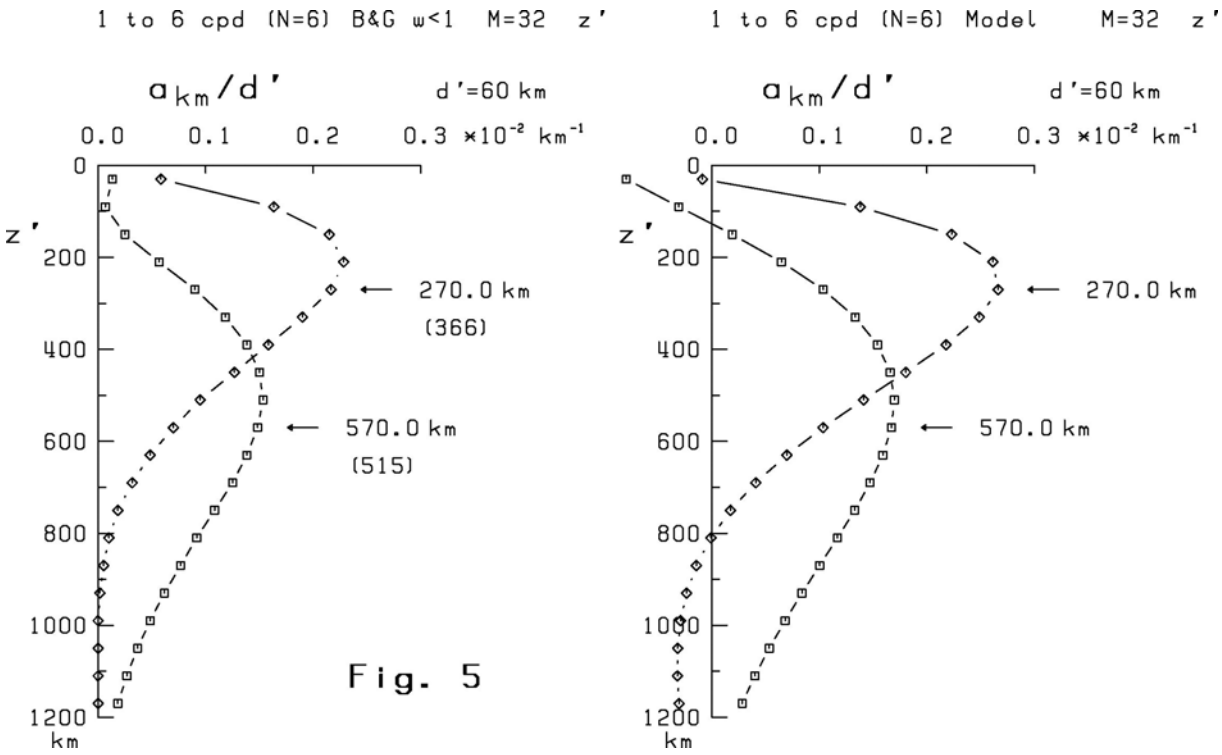

Fig. 5

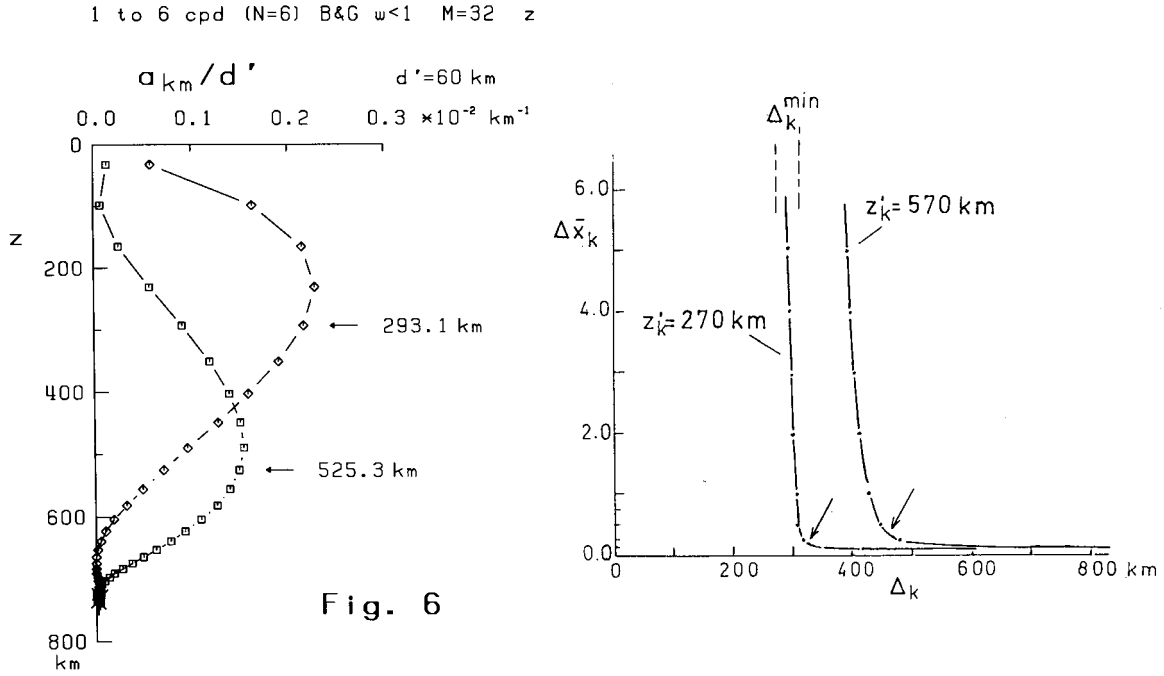

Fig. 6

We conclude by considering various possibilities to improve the resolution power of 1D sounding. Increasing the number of response estimates with a closer spacing in frequency improves accuracy, but not resolution, which means that we have to expand the frequency range beyond the decade of daily variations. To this end we add hypothetical responses for two more decades, again with six estimates per decade, extending from 10 to 60 cpd for substorm variations and from 0.1 to 0.6 for smoothed storm-time variations. This gives 18 responses for periods ranging from 24 minutes to 10 days. The resulting resolution curves are

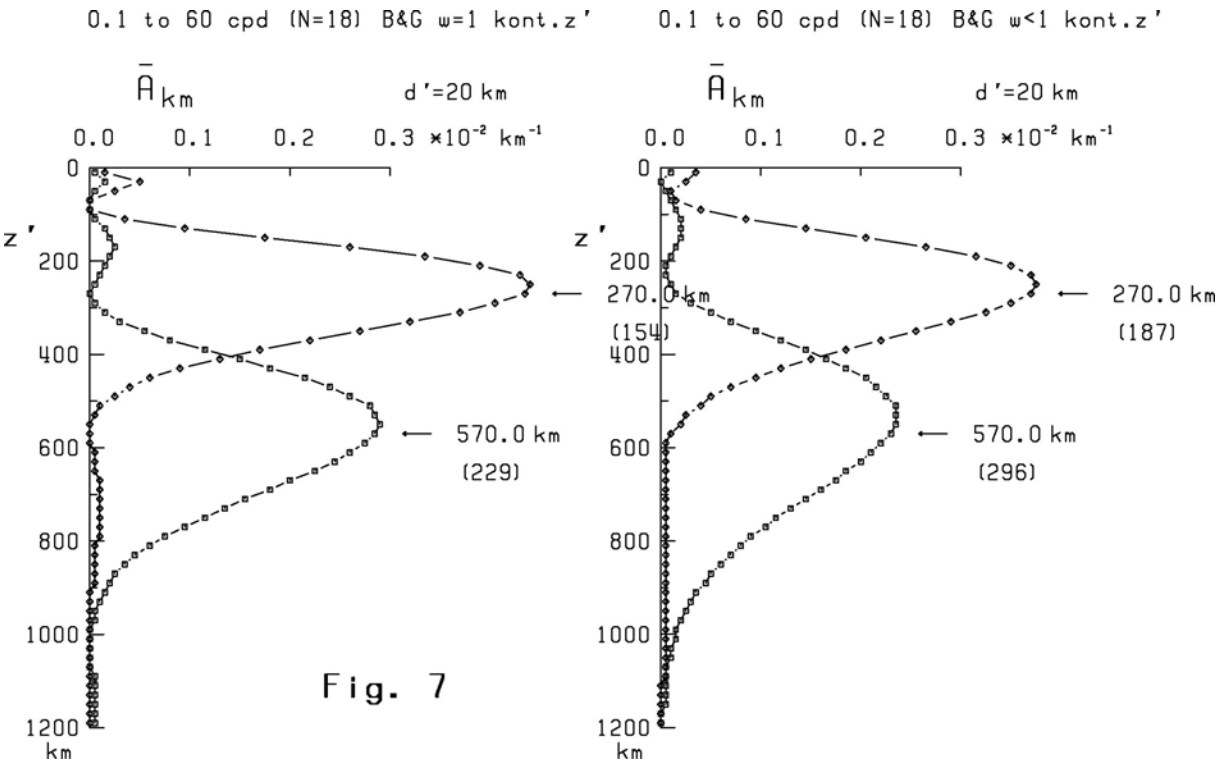

shown in **Fig. 7**. The curve to the left is for exact data and the curve to the right for error-bearing data. We assume thereby that all data have the above stated errors of daily variations, and we adjust the trade-off parameter again to yield at target depth the same model errors as the 32-layer model. Continuous models are assumed with model-independent approximated data kernels as for the left display in Fig. 4. This enlargement of the data basis improves the resolution indeed substantially and averaging depths are now small enough that structural details become visible, when their extent in depth is at least comparable with the spreads of 187 and 296 km, respectively.

We address finally in the same way two specific questions, whether EM soundings could detect a frequently postulated asthenospheric conductor and also a proposed mid-mantle conductor at about 800 km depth. Therefore we test now their resolution at z' target depths of 150 km and 810 km, and by changing the scaling resistivity ρ_0 from $70\,\Omega\,\mathrm{m}$ to $1\,\Omega\,\mathrm{m}$ for the mid-mantle, we can expect that from, say, 700 *km* downwards z' correspond to true depth except for a certain off-set due to the more resistive uppermost mantle. We proceed once more from 18 responses over three decades and assume for them that they have the same errors as daily variations. Noting that the first target depth corresponds to the third layer of the 32-layer model and the second to its fourteenth layer, the trade-off parameter are adjusted again to yield the modelling errors of these layers.

For the study of the asthenosphere we add six responses from 100 to 600 cpd for slow pulsations to those of substorms and daily variations. For the mid-mantle conductor we add six responses for the long-periodic Dst continuum from 0.01 to 0.06 cpd to those for smoothed storm-time and daily variations. Thus periods extend from 144 seconds to one day and from 4 hours to 100 days, respectively. As **Fig. 8** shows, we have achieved now a nearly delta-shaped response for the upper mantle, even though the averaging depth still measures 100 km. Furthermore, the mantle below 750 km has come within the reach of EM soundings, with an acceptable spread of less than 400 km. The overall conclusion is that both conducting zones, if they exist, could be detected, even though in case of the asthenophere a possible

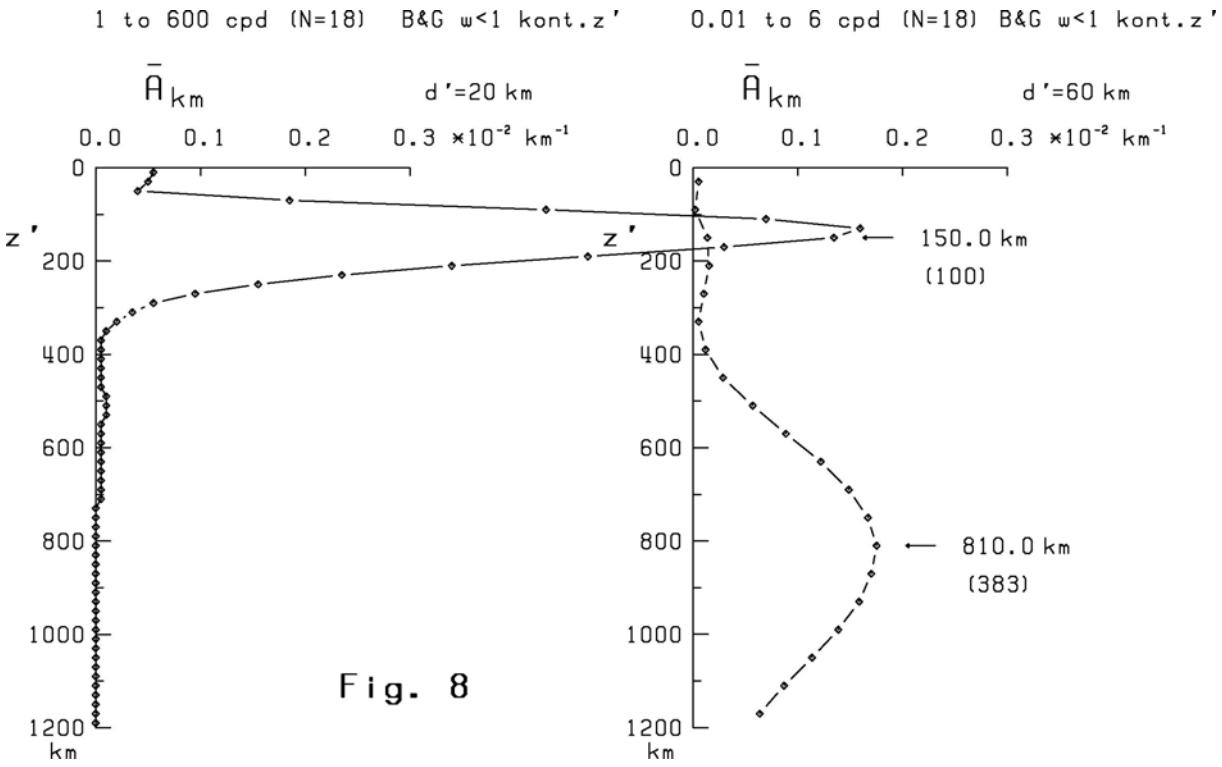

Fig. 8

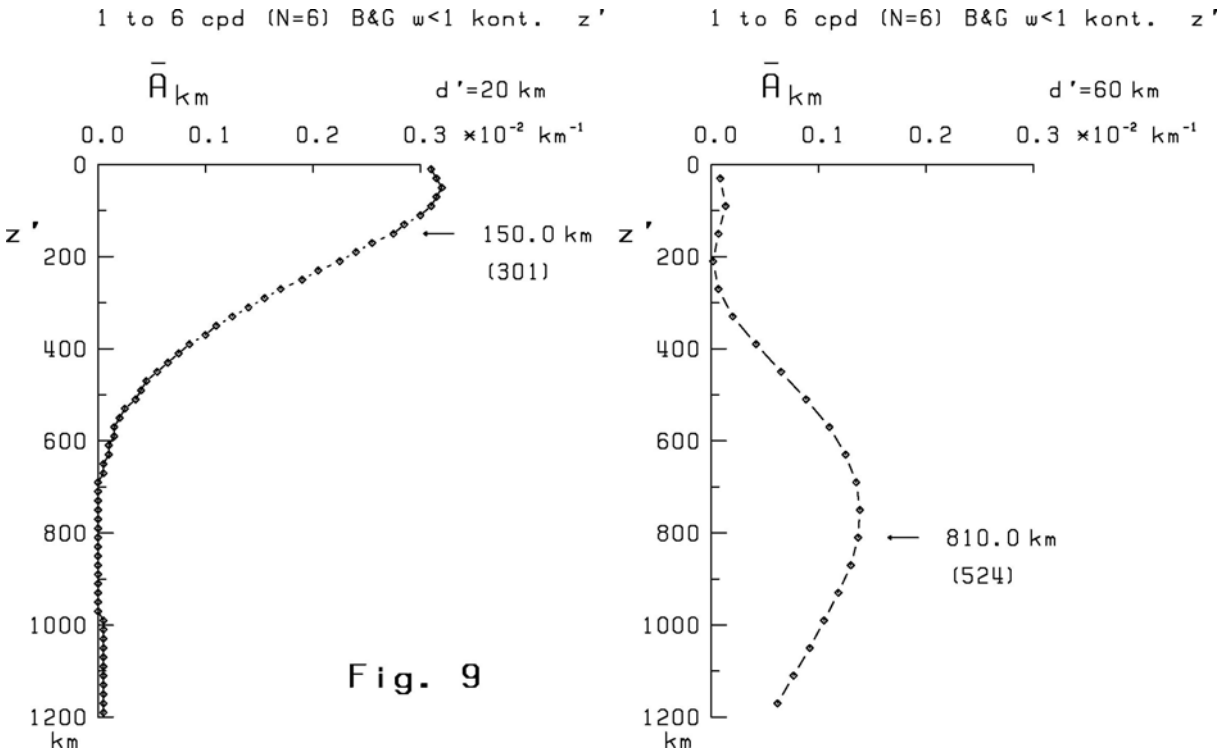

Fig. 9

screening by a surface or crustal conductor has not been taken into account yet. It would require further studies with an exact data kernel for preconceived models.

Fig. 9 complements Fig. 8 by demonstrating the loss of resolution, when responses are restricted again to the six harmonics of daily variations. We note that the two target depths are then outside their z*-depth range from 330 km to 660 km. Therefore any modelling result for the asthenosphere would represent an average over the entire crust and upper mantle, while for the mid-mantle target depth the spread has increased to more than 500 km.

References

Berdichevsky, M.N. & V.I.Dmitriev, 2002. Magnetotellurics in the context of the theory of ill-posed problems. *Investigations in Geophysics No.***11**. Soc. Exploration Geophysicists, Tulsa, Oklahoma, 215 pp.

Bibby, H.M., T.G. Caldwell & C. Brown, 2005. Determinable and non-determinable parameter of galvanic distortion in magnetotellurics. *Geophys. J. Int.*, **163**. 915-930.

Constable, S.C., R.L. Parker & C.G. Constable, 1987. Occam's inversion: A practical algorithm for generating smooth models from electromagnetic sounding data. *Geophysics*, **52,** 289-300.

Eckhardt, D., 1968. Theory and interpretation of the electromagnetic impedance of the Earth. *J. Geophys. Res.*, **73**, 5317-5326.

Haak, V., 1978. Interpretations-Verfahren für die Magnetotellurik unter besonderer Berücksichtigung lateral variierender elektrischer Leitfähigkeiten im Erdinnern und eines räumlich inhomogenen induzierenden Magnetfeld. *Bayerische Akad. Wissenschaften, Math-nat. Klasse,* Abhandl. Neue Folge, Heft **158**.

Kress, R.. 1991. Numerical analysis. Springer-Verlag, New York, 326 pp.

Lahti, L., T. Korja, P. Kaikkonen, K. Vaittinen & BEAR Working Group, 2005. Decomposition analysis of the BEAR magnetotelluric data: implications for the upper mantle conductivity in the Fennoscandian Shield. *Geophys. J. Int.*, **163.** 900-914.

Larsen, J.C., 1975. Low frequency (0.1-6.0 cpd) electromagnetic study of deep mantle electrical conductivity beneath the Hawaiian Islands. *Geophys. J. R. astr. Soc.*, **3**, 17-46.

Parker, R.l., 1994. Geophysical inverse theory. *Princeton University Press*, Princeton, NJ., 386 pp.

Parker, R.L. & J.R. Booker, 1996. Optimal one-dimensional inversion and and bounding of magnetotelluric apparent resistivity and phase measurements. *Phys. Earth Plan. Int.*, 98, 269-282.

Schmucker, U.,1974. Erdmagnetische Tiefensondierung mit langperiodischen Variationen. *Kolloquium Erdmagnetische Tiefensondierung Grafrath*, 313-342.

Schmucker, U., 2001. Zur Analyse erdmagnetischer und erdelektrischer Daten- neue Fassung älterer Programme. *Kolloquium Elektromagnetische Tiefenforschung Ludwigstein*, 220-251.

Schmucker, U. & P. Weidelt, 1975. Electromagnetic induction in the Earth.Lecture Notes Aarhus (unpublished manuscript),

Weidelt, P., 1972. The inverse problem of geomagnetic induction. *Z. f. Geophys.*,***38**, 257-289.*

Weidelt, P., 1986. Discrete frequency inequalities for magnetotelluric impedances of one-dimensional conductors. *Z. f. Geophys., 59, 171-176.*

Whittall, K.P. & D.W. Oldenburg, 1992. Inversion of magnetotelluric data for a one -dimensional conductivity. *Geophys. Monogr. Series* No. **5**. Soc. Exploration Geophysicists, Tulsa, Oklahoma, 114 pp.

Appendix A. The Psi-alorithm

We assume induction in a layered plane model of *M* layers by a quasi-uniform TE field and proceed from the solution of the 1D diffusion equation $d^2E_x/dz^2 = i\omega\mu_0/\rho \cdot E_x$ for the electric field E_x at depth *z* within the *m*-th layer. With $K_m = \sqrt{i\omega_n\mu_0/\rho_m}$ for angular frequency ω_n and z_m as depth to the top of this layer

$$E_x(z) = A_m \exp\{-K_m(z - z_m)\} + B_m \exp\{+K_m(z - z_m)\} \ .$$

With $B_y = -\frac{dE_x}{dz}/i\omega$ as magnetic field, a thus defined C-response $C = E_x/i\omega B_y$ yields

$$C_m = \frac{1}{K_m}\frac{1+U_m}{1-U_m} \qquad \text{with } U_m = B_m/A_m$$

for the top $z = z_m$ of the *m*-th layer and

$$C_m^+ = \frac{1}{K_m}\frac{1+U_m^+}{1-U_m^+} \quad \text{with} \quad U_m^+ = U_m \exp\{2K_m d_m\} .$$

for the bottom $z = z_{m+1} = z_m + d_m$. Introducing $\Psi = 2\ln(KC)$ as logarithmic response, we obtain for $z = z_m$

$$\Psi_m = 2\ln\{K_m C_m\} = 4\tanh^{-1}\{U_m\}$$

with a corresponding expression for the bottom. According to eq. (2) we replace now $K_m d_m$ by $\alpha_n d'$ for an evenly subdivided model in z' depth, with d' as constant layer thickness; $\alpha_n = \sqrt{i\omega_n\mu_0/\rho_0}$, where ρ_0 denotes the scaling resistivity. Then the thus defined γ-ratio of the logarithmic responses at the top and bottom in terms of U_m^+ is

$$\gamma_m = \frac{\Psi_m}{\Psi_m^+} = \frac{\tanh^{-1}\{U_m^+ \cdot \exp\{-2\alpha_n d'\}}{\tanh^{-1}\{U_m^+\}} \quad . \tag{A1}$$

The absolute value $|U_m^+|$ never exceeds unity and remains near to zero, provided the changes of resistivity from layer to layer are moderate with, say, $|\ln(\rho_{m+1}/\rho_m)| \le 2.3$. Then to second order in $|U_m^+|$ the γ-ratio can be approximated by

$$\gamma_m = \exp\{-2\alpha_n d'\} \tag{A2}$$

for all layers. Continuity of the C-response across layer boundaries implies $C_m^+ = C_{m+1}$ or in terms of the logarithmic responses $\Psi_m^+ = \Psi_{m+1} + \ln(K_m / K_{m+1})$, which in combination with eq. (A2) gives

$$\Psi_m = \gamma_m \Psi_m^+ = \gamma_m \{\Psi_{m+1} + x_{m+1} - x_m\}, \tag{A3}$$

with $x = \ln(\rho/\rho_0)$ from eq. (9).
The Psi-algorithm starts with $\Psi_M = 0$ on the surface of the underlying uniform half-space at depth $z = z_M$, with $B_M = 0$ and thereby also $U_M = 0$. Then from eq. (A3)

$$\Psi_{M-1} = \gamma_{M-1} \cdot (x_M - x_{M-1}), \quad \Psi_{M-2} = \gamma_{M-2}\gamma_{M-1} x_M + \gamma_{M-2}(1-\gamma_{M-1}) x_{M-1} - \gamma_{M-2} x_{M-2} \ , \ \ldots\ldots ,$$

$$\Psi_1 = \gamma_1\gamma_2 \ldots \gamma_{M-1} x_M + \gamma_1\gamma_2 \ldots \gamma_{M-2}(1-\gamma_{M-1}) x_{M-1} + \ldots\ldots + \gamma_1(1-\gamma_2) x_2 - \gamma_1 x_1 \ .$$

We connect now the surface value Ψ_1 to the response y_n as defined in eq. (8). With $C_1 = C(\omega_n)$ as surface value of the C-response, $K_1 = \sqrt{i\omega_n \mu_0 / \rho_1}$ and α_n from above we obtain $\Psi_1 = 2\ln\{K_1 C_1\} = 2\ln\{\alpha_n C(\omega_n)\} - x_1 = y_n^{\mathrm{mod}} - x_1$ with $y_n^{\mathrm{mod}} = \Psi_1 + x_1$ denoting the response of the model. Adding then x_1 to Ψ_1 changes the last term from $-\gamma_1 x_1$ to $(1-\gamma_1) x_1$ and the forward problem to find the response for a given model takes the form of the quasi-linear functional of eq. (5) :

$$y_n^{\mathrm{mod}} = \sum_{m=1}^{M} g_{nm}\, x_m \qquad \text{with} \qquad g_{nm} = \gamma_1\gamma_2 \ldots \gamma_{m-1}(1-\gamma_m) \tag{A4}$$

as data kernel, setting $\gamma_0 = 1$ and $\gamma_M = 0$. When the use of the approximated γ-ratio from eq. (A2) can be justified for all layers, we obtain the model-independent approximation

$$g_{nm}^{(0)} = \exp\{-2\alpha_n (m-1) d'\} - \exp\{-2\alpha_n m d'\} = \exp\{-2\alpha_n z_m'\} \cdot \sinh(\alpha_n d'), \tag{A5}$$

with $z_m' = (m - 1/2) d'$ as depth of the centre of the *m*-th layer, for starting the iterative process for 1D modelling, as outlined in Section 2.

When the model parameter x_m is replaced by $u_m = x_m - x_{m-1}$ according to eq. (10) to express the change of resistivities from layer to layer, with $x_0 = 0$, eq. (A3) changes into

$$\Psi_m = \gamma_m(\Psi_{m+1} + u_{m+1}) \tag{A6}$$

and the Psi-algorithm in terms of u_m into

$$\Psi_{M-1} = \gamma_{M-1} \cdot u_M\,, \quad \Psi_{M-2} = \gamma_{M-2}\gamma_{M-1}u_M + \gamma_{M-2}u_{M-1}\,, \quad \ldots\ldots\,,$$

$$\Psi_1 = \gamma_1\gamma_2\ldots\gamma_{M-1}u_M + \gamma_1\gamma_2\ldots\gamma_{M-2}u_{M-1} + \ldots\ldots + \gamma_1\gamma_2 u_3 + \gamma_1 u_2\,.$$

With $u_1 = x_1$ the new quasi-linear functional for the forward problem follows as

$$y_n^{\mathrm{mod}} = \Psi_1 + u_1 = \sum_{m=1}^{M} \hat{g}_{nm}\, u_m \quad \text{with} \quad \hat{g}_{nm} = \gamma_1\gamma_2\ldots\gamma_{m-1} \tag{A7}$$

as data kernel, setting again $\gamma_0 = 1$. Their model-independent approximation is

$$\hat{g}_{nm} = \exp\{-2\alpha_n(m-1)d'\} = \exp\{-2\alpha_n(z'_m - d'/2)\} \tag{A8}$$

in the same notations as in eq. (A5).

Appendix B. Invariance of solutions against the choice of the scaling resistivity ρ_0

We test whether the solution $y_n^{\mathrm{mod}} = \sum_m g_{nm}\, x_m$ of the forward problem depends on the chosen scaling resistivity ρ_0. A change to a new value ρ'_0 means that the constant $c = \ln\{\rho_0/\rho'_0\}$ is added to the data and to the model parameter, i.e. y_n^{mod} is changed to $y'^{\mathrm{mod}}_n = y_n^{\mathrm{mod}} + c$ and x_m to $x'_m = x_m + c$. The data kernel remains the same, provided that the ratio $d_m/\sqrt{\rho_m}$ in eq. (2) is kept constant by replacing d' by $d'' = d'\sqrt{\rho'_0/\rho_0}$. Then as seen from the condition

$$y'^{\mathrm{mod}}_n = \sum_m g_{nm}\,(x_m + c) = y_n^{\mathrm{mod}} + c\,,$$

invariance against the choice of ρ_0 implies that $\sum_m g_{nm}$ equals unity. Eq. (A4) shows in

$$\sum_m g_{nm} = 1 - \gamma_1 + \gamma_1(1-\gamma_2) + \ldots\ldots + \gamma_1\gamma_2\ldots\gamma_{M-2}(1-\gamma_{M-1}) + \gamma_1\gamma_2\ldots\gamma_{M-1} = 1 \tag{B1}$$

that this is the case. Invariance should apply then to the solution of the inverse problem as well, which has the following consequence: Under the stated condition for the data kernel also

the solution coefficients h_{kn} remain the same. Then invariance of the solution $\vec{x}_k = \sum_n h_{kn} y_n$ requires that $\vec{x}'_k = \sum_n h_{kn}(y_n + c) = \vec{x}_k + c$ which implies that $\sum_n h_{kn} = 1$ and thereby that

$$\sum_m a_{km} = \sum_m \sum_n h_{kn} g_{nm} = \sum_n h_{kn} \sum_m g_{nm} = \sum_n h_{kn} = 1 \ , \qquad \text{(B2)}$$

which is readily identified as the added condition of eq. (34) in the Backus & Gilbert theory.

Replacing the model parameter x_m by $u_m = x_m - x_{m-1}$, with $x_0 = 0$ and thus $u_1 = x_1$, the forward problem to be solved becomes $y_n^{\mathrm{mod}} = \sum_m \hat{g}_{nm} u_m$. The change from ρ_0 to ρ'_0 changes only u_1 to $u'_1 = u_1 + c$, while $u'_m = u_m$ for $m = 2,3,..$ remain the same. We presume that d' has been properly changed to d'' to have unchanged data kernels. Invariance against the choice of ρ_0 requires in

$$y_n'^{\mathrm{mod}} = \hat{g}_{n1}(u_1 + c) + \sum_{m=2}^{M} \hat{g}_{nm} u_m = \sum_{m=1}^{M} \hat{g}_{nm} u_m + \hat{g}_{n1} \cdot c = y_n^{\mathrm{mod}} + c$$

that $\hat{g}_{n1}$ equals unity, which is the case as evident from eq. (A7), while invariance of the inverse solution $\vec{u}_k = \sum_n \hat{h}_{kn} y_n$ leads in

$$\vec{u}'_1 = \vec{u}_1 + c = \sum_n \hat{h}_{1n}(y_n + c) \quad \text{and} \quad \vec{u}'_k = \vec{u}_k = \sum_n \hat{h}_{kn}(y_n + c) \ \text{ for } k = 2,3,.. \text{ to}$$

$$\sum_n \hat{h}_{1n} = 1 \quad \text{and} \quad \sum_n \hat{h}_{kn} = 0 \ \text{ for } k = 2,3,.... \qquad \text{(B3)}$$

in analogy to eq. (B1). Then with $b_{\hat{n}n} = \sum_{k=1}^{M} \hat{g}_{\hat{n}k} \hat{h}_{kn}$ as element of matrix $\underline{\underline{B}} = \underline{\underline{G}}\,\underline{\underline{H}}$

$$\sum_n b_{\hat{n}n} = \sum_{k=1}^{M} \hat{g}_{\hat{n}k} \sum_n \hat{h}_{kn} = \hat{g}_{\hat{n}1} = 1 \qquad \text{(B4)}$$

in analogy to eq. (B2). Furthermore it is readily verified that this equation applies also, when the model parameter is x_m, and the same turns out to be approximately correct for eq. (B2) in conjunction with u_m as model parameter.

We conclude firstly that the choice of ρ_0 has no influence upon the modelling results, and secondly that the elements of the resolution and information density matrix in given rows act like numerical filters upon model or data at the respective target depth or frequency, with the sum of filter weights being equal to unity.

Appendix C. Differentiations with respect to the regularisation parameter α

In order to simplify notations lower case letters are vectors and upper case letters matrices. Furthermore, the bar above the vector $\underline{\vec{x}}$ of the averaged model is omitted. With

$P = G^T G + \alpha I_M$ the pseudo-inverse of eq. (21) leads with eq. (14) to $x = P^{-1} G^T y$ and $x^T = y^T G P^{-1}$, with $(P^{-1})^T = P^{-1}$. Differentiation of P^{-1} with respect to α yields

$$\frac{dP^{-1}}{d\alpha} = -P^{-1}\frac{dP}{d\alpha}P^{-1} = -P^{-1} I_M P^{-1}$$

(cf. Parker, 1994; eq. 30 in Section 3.02). Then

$$\frac{\partial x^T x}{\partial \alpha} = -y^T G P^{-1} P^{-1} x - x^T P^{-1} P^{-1} G^T y = -2 \cdot x^T P^{-1} x \ .$$

The squared misfit residual norm to be differentiated next is

$$\delta y^T y = (y - Gx)^T (y - Gx) = y^T y - x^T G^T y - y^T G x + x^T G^T G x \ .$$

Rewriting eq. (21) in the form $(G^T G + \alpha I_M) x = G^T y$ yields $G^T G x = G^T y - \alpha x$ and thereby

$$\delta y^T \delta y = y^T y - y^T G x - \alpha \cdot x^T x \qquad \text{(C1)}$$

which represents a convenient formula to derive this squared norm. Differentiation with respect to α yields

$$\frac{\partial (\delta y^T \delta y)}{\partial \alpha} = y^T G P^{-1} P^{-1} G^T y - x^T x + \alpha \cdot (y^T G P^{-1} P^{-1} x + x^T P^{-1} P^{-1} G^T y) = x^T x - x^T x + 2\alpha \cdot x^T P^{-1} x$$

The final results in full notations are

$$\frac{\partial \underline{\vec{x}}^T \underline{\vec{x}}}{\partial \alpha} = -2 \cdot \underline{\vec{x}}^T (\underline{\underline{G}}^T \underline{\underline{G}} + \alpha I_M)^{-1} \underline{\vec{x}} \quad \text{and} \quad \frac{\partial y^T y}{\partial \alpha} = +2\alpha \cdot \underline{\vec{x}}^T (\underline{\underline{G}}^T \underline{\underline{G}} + \alpha I_M)^{-1} \underline{\vec{x}} \ . \qquad \text{(C2)}$$

Appendix D. The determination of spread Δ_k in the Backus & Gilbert theory

Insertion of a_{km} from eq. (16) and of $A_k(z')$ from eq. (29) into the definitions for the spread in eq. (25), multiplied with d' for a dimensioned quantity, and eq. (30), respectively, gives

$$\Delta_k = d' \sum_m \sum_{\hat{n}} h_{k\hat{n}} \sum_n h_{kn} g_{\hat{n}m} g_{nm} J_{km} \quad \text{and} \quad \Delta_k = \int_0^\infty \sum_{\hat{n}} h_{k\hat{n}} \sum_n h_{kn} G_{\hat{n}}(z') G_n(z') J_k(z') dz' \ .$$

After changing the sequence of summations or the sequence of integration and summations, these expressions are reduced to

$$\Delta_k = \sum_{\tilde{n}} h_{k\hat{n}} \sum_n h_{kn} b_{n\hat{n}} \qquad \text{(D1)}$$

with $b_{n\hat{n}}$ as defined in eq. (35) for discrete and continuous models. Excluding the case $w = 0$, eq. (39) yields

$$\sum_n h_{kn} b_{n\hat{n}} = -\frac{1}{w}\left[\lambda_k + (1-w)\, s_0^2\, h_{k\hat{n}}\right]$$

and together with eq. (D1) the relation

$$\Delta_k = -\frac{1}{w}\left\{\lambda_k \sum_{\hat{n}} h_{k\ddot{n}} + (1-w)\, s_0^2 \sum_{\hat{n}} h_{k\hat{n}}^2\right\}.$$

With $\sum_n h_{kn} = 1$ according to eqs (33) and (34) and with $s_0^2 \sum_n h_{kn}^2 = \Delta\vec{x}_k^2$ from eq. (18) we obtain for the spread of trade-off models

$$\Delta_k = -\frac{\lambda_k}{w} - \frac{1-w}{w}\Delta\vec{x}_k^2, \qquad \text{(D2)}$$

and thus for the spread of minimum spread models with $w = 1$

$$\Delta_k = -\lambda_k \ . \qquad \text{(D3)}$$

Insertion of $h_{kn} = 1/2N$ from to eq. (37) for $w = 0$ yields finally the spread of minimum variance models in

$$\Delta_k = \frac{1}{4N^2}\sum_{\hat{n}}\sum_n b_{n\ddot{n}} \ . \qquad \text{(D4)}$$